J. Nonlinear Sci. Vol. 11: pp. 3–45 (2001)
DOI: 10.1007/s003320010009

Journal of
Nonlinear
Science

On the Dynamics of Elastic Strips

A. Goriely,[1] M. Nizette,[2] and M. Tabor[1]

[1] University of Arizona, Department of Mathematics and Program in Applied Mathematics, Building 89, Tucson, AZ 85721, USA
E-mail: goriely@ math.arizona.edu

[2] Université Libre de Bruxelles, Theoretical Nonlinear Optics CP231, Bruxelles, Belgium

Received February 16, 1999; accepted October 24, 2000
Online publication February 20, 2001
Communicated by Philip Holmes

Summary. The dynamics of elastic strips, i.e., long thin rods with noncircular cross section, is analyzed by studying the solutions of the appropriate Kirchhoff equations. First, it is shown that if a naturally straight strip is deformed into a helix, the only equilibrium helical configurations are those with no internal twist and whose principal bending direction is either along the normal or the binormal. Second, the linear stability of a straight twisted strip under tension is analyzed, showing the possibility of both pitchfork and Hopf bifurcations depending on the external and geometric constraints. Third, nonlinear amplitude equations are derived describing the dynamics close to the different bifurcation regimes. Finally, special analytical solutions to these equations are used to describe the buckling of strips. In particular, finite-length solutions with a variety of boundary conditions are considered.

Key words. elastic strips, amplitude equations, localized solutions

1. Introduction

Filamentary structures can be observed in nature at all scales from microscopic chains of molecules to macroscopic braided magnetic flux tubes in solar flares. Remarkably, despite their different length scales and microscopic structures, unstable filaments seem to follow universal configurational changes triggered by generic instabilities. A simple everyday experiment is the coiling of strings, ropes, or telephone cords: If one holds the ends of a piece of rubber tubing and twists one end relative to the other, the string will soon coil up on itself. This is a simple example of a *writhing instability*, or *twist-to-writhe* conversion, in which a local change in twist density eventually results in a global reconfiguration

of the string.[1] Understanding the onset and dynamics of this fundamental instability is of both theoretical and practical interest since it lies at the heart of a host of important processes. Engineers have needed to understand the instabilities of rods to prevent the pop-out of cables—especially in the case of suboceanic cables [42]. In biology, elastic filaments provide idealized models with which to study the coiling behavior of different filamentary structure such as those of proteins, polymers, DNA, and bacterial fibers [3], [4], [5], [21], [33], [35], [41]. In physics there are many different settings where long, thin, and twisted structures play an important role, such as the motion of vortex tubes in hydrodynamics [22]; the formation of sun spots and the heating of the solar corona [11], [37]; the theory of polymers and liquid crystals [14], [34]. More recently, interesting connections between curve dynamics and integrable hierarchies of partial differential equations have been unraveled [13], [23], [25], [28].

However, a complete mathematical model of the dynamics of even the simplest writhing instability has proved to be difficult to obtain. The simplest mechanical formulation that can capture the correct three-dimensional geometry and dynamics of this problem is provided by the *Kirchhoff equations* for thin elastic rods. Virtually all of the analysis of the Kirchhoff model has been restricted to the stationary, i.e., time-independent, solutions [27], [31], [35] and only a few time-dependent problems have been tackled.

Recently we have developed a new method [16], [17], [18], [19] to study the dynamics of filaments by introducing a novel perturbation scheme. Starting from a stationary solution of Kirchhoff's equation, this scheme allows us to derive a dispersion relation from which one can determine the stability, or lack thereof, of the stationary solution. This provides a simple and direct way to test the stability of the filament under perturbation. Once an instability is triggered, the dynamics of the filament can become extremely complicated. Nevertheless, a nonlinear analysis of the solution after bifurcation can be carried out by deriving amplitude equations that describe the behavior of the filament beyond the instability threshold [15], [17], and we derived such equations for thin elastic rods with circular cross sections.

The goal of this paper is to extend our earlier work [17] to the case of rods with an asymmetric cross section (referred to, in this paper, as *strips*). A linear analysis of the static Kirchhoff equations for straight strips was performed for the first time in Champneys and Thompson (1996) [6] followed by a normal form analysis in van der Heijden and Thompson (1998) [40]. First, we show that the class of exact helical solutions of the Kirchhoff equations for strips is much more restricted than those for symmetric rods. This emphasizes the highly degenerate character of the latter case. Second, two different regimes of bifurcation of twisted straight strips are identified, in accordance with [6], depending on the values of the parameters characterizing the elasticity of the material and the geometry of the cross section. The dynamics of strips exhibits behaviors that are significantly different from the case of rods with circular cross sections. In Section 3, which focuses on the dynamical character of the instabilities, we linearize the time-dependent equations and identify particular modes of wave propagation. We also look for the critical point in parameter space beyond which a straight strip becomes unstable and

[1] The word *writhe* is used to denote a global deformation of a filamentary structure.

recover the results of [6]. In Section 4, we derive time-dependent amplitude equations from the Kirchhoff equations in a regime where the system is close to bifurcation, complementing the normal form analysis performed in [40]. Expressions for physical quantities of interest in terms of the new variables are computed. In Section 5, we discuss in detail static solutions of the resulting amplitude equations, and we consider finite-length solutions to practical problems of interest. The buckling mode stability is discussed too. We find that strips may adopt different bifurcation paths, depending not only on the nature of the boundary conditions, but also, in some cases, on the material elasticity and cross section geometry.

2. The Kirchhoff Model

The Kirchhoff model accounts for the dynamics of a thin elastic rod subject to internal stresses and boundary constraints. In this model, the elastic stresses are averaged over the rod cross sections (which are assumed to be small relative to the length of the rod) along the space curve describing the rod centerline. This results in a one-dimensional model that incorporates both the bending and twisting motions of the rod. The twisting motion, as will be described below, is conveniently interpreted as the winding of a ribbon about the axial curve.

2.1. Space Curves and Ribbons

We consider a dynamical *space curve* $\mathbf{R}(s,t)$ parameterized by its arclength s and time t. A *ribbon* is defined as a space curve $\mathbf{R}(s,t)$ together with a smooth unit vector field $\mathbf{d}_2(s,t)$ orthogonal to that curve. Utilizing the unit tangent vector, $\mathbf{d}_3 \equiv \mathbf{t}$, we can form a third unit vector $\mathbf{d}_1 = \mathbf{d}_2 \times \mathbf{d}_3$, so that the *general triad* $(\mathbf{d}_1, \mathbf{d}_2, \mathbf{d}_3)$ forms a right-handed orthonormal basis. This basis is a generalization of the Frenet triad $(\mathbf{n}, \mathbf{b}, \mathbf{t})$ accounting for the additional data in the definition of the ribbon. The components of the derivatives of the general triad $\mathbf{d}_1$, $\mathbf{d}_2$, and $\mathbf{d}_3$ with respect to arclength s and time t are expressed in the local basis form, respectively, the *twist matrix* $\mathbf{K}(s,t)$ and the *spin matrix* $\mathbf{W}(s,t)$, which we define as follows:

$$\begin{pmatrix} \frac{\partial \mathbf{d}_1}{\partial s} & \frac{\partial \mathbf{d}_2}{\partial s} & \frac{\partial \mathbf{d}_3}{\partial s} \end{pmatrix} \equiv \begin{pmatrix} \mathbf{d}_1 & \mathbf{d}_2 & \mathbf{d}_3 \end{pmatrix} \mathbf{K}, \tag{1.a}$$

$$\begin{pmatrix} \frac{\partial \mathbf{d}_1}{\partial t} & \frac{\partial \mathbf{d}_2}{\partial t} & \frac{\partial \mathbf{d}_3}{\partial t} \end{pmatrix} \equiv \begin{pmatrix} \mathbf{d}_1 & \mathbf{d}_2 & \mathbf{d}_3 \end{pmatrix} \mathbf{W}. \tag{1.b}$$

These matrices are antisymmetric and can be written as

$$\mathbf{K} \equiv \begin{pmatrix} 0 & -\kappa_3 & \kappa_2 \\ \kappa_3 & 0 & -\kappa_1 \\ -\kappa_2 & \kappa_1 & 0 \end{pmatrix}, \qquad \mathbf{W} \equiv \begin{pmatrix} 0 & -\omega_3 & \omega_2 \\ \omega_3 & 0 & -\omega_1 \\ -\omega_2 & \omega_1 & 0 \end{pmatrix}. \tag{2}$$

The entries of $\mathbf{K}$ and $\mathbf{W}$ are not independent. By differentiating (1.a) with respect to time and (1.b) with respect to arclength and then equating their cross derivatives, we obtain

a compatibility relation for $\mathbf{K}$ and $\mathbf{W}$,

$$\frac{\partial \mathbf{K}}{\partial t} - \frac{\partial \mathbf{W}}{\partial s} = [\mathbf{K}, \mathbf{W}], \tag{3}$$

where $[\mathbf{K}, \mathbf{W}] = \mathbf{KW} - \mathbf{WK}$. The components κ_i and ω_i form the *twist vector* $\kappa = \kappa_1 \mathbf{d}_1 + \kappa_2 \mathbf{d}_2 + \kappa_3 \mathbf{d}_3$ and the *spin vector* $\omega = \omega_1 \mathbf{d}_1 + \omega_2 \mathbf{d}_2 + \omega_3 \mathbf{d}_3$.

The equations (1.a) constitute the generalization of the Frenet-Serret equations for the ribbon. The component κ_3 is called the *twist density* and defines the amount of rotation of the local basis ($\mathbf{d}_1$, $\mathbf{d}_2$, $\mathbf{d}_3$) around the tangent vector $\mathbf{d}_3$ as the arc length s increases. The twist vector components can be expressed as functions of the angle ζ between the vector $\mathbf{d}_1$ and the normal $\mathbf{n}$ to the curve, the Frenet curvature κ, and the torsion τ:

$$(\kappa_1, \kappa_2, \kappa_3) = \left(\kappa \sin \zeta, \kappa \cos \zeta, \tau + \frac{\partial \zeta}{\partial s} \right). \tag{4}$$

The quantities τ, $\frac{\partial \zeta}{\partial s}$, and κ_3 play related but distinct roles. The *torsion* τ is a property of the curve alone and is a measure of its nonplanarity. Hence, a curve with null torsion is a plane curve, and any two ribbons having the same curvature and torsion for all s and t correspond to the same space curve $\mathbf{R}$ and can only be distinguished by the orientation of the local basis. The *intrinsic twist density* $\frac{\partial \zeta}{\partial s}$ is a property of the ribbon alone, representing the rotation of the local basis with respect to the Frenet frame as the arc length increases. A ribbon without intrinsic twist is called a *Frenet ribbon*. Indeed, in a Frenet ribbon, the angle ζ between the binormal $\mathbf{b}$ and the vector field $\mathbf{d}_2$ is constant; hence the binormal is representative of the orientation of the local basis ($\mathbf{d}_1$, $\mathbf{d}_2$, $\mathbf{d}_3$). The *total twist density*, κ_3, is a property of both the space curve and the ribbon, measuring the total rotation of the local basis around the space curve as the arc length increases.

2.2. The Kirchhoff Equations

The central idea of the model is that the rod is modeled as a sequence of contiguous segments between which the forces and moments are determined. The required assumptions are: (i) the rod is *thin*, i.e., the width of any cross section is much smaller than any other length scale (e.g., $|\kappa|^{-1}$) involved in the problem; (ii) the rod is unshearable and inextensible, i.e., each cross section remains normal to the axial space curve and can be identified by its arclength coordinate; (iii) the elastic stresses are linear in the strains. A detailed derivation of the Kirchhoff equations can be found in [2], [8]. More general models, including the effects of shear deformations and extensibility [1], as well as nonlinear constitutive elastic laws [27], can also be considered.

By averaging the forces and moments over each cross section, one can obtain the equations for the force, $\mathbf{F}(s, t)$, acting on each cross section, and for the moment $\mathbf{M}(s, t)$. These equations are closed by using the constitutive relation of linear elasticity relating the torque $\mathbf{M}$ to the twist vector κ. Together, they read:

$$\mathbf{F}'' = \xi \mathcal{A} \ddot{\mathbf{d}}_3, \tag{5.a}$$

$$\mathbf{M}' + \mathbf{d}_3 \times \mathbf{F} = \xi \left(I_2 \mathbf{d}_1 \times \ddot{\mathbf{d}}_1 + I_1 \mathbf{d}_2 \times \ddot{\mathbf{d}}_2 \right), \tag{5.b}$$

$$\mathbf{M} = E I_1 \kappa_1 \mathbf{d}_1 + E I_2 \kappa_2 \mathbf{d}_2 + \mu J \kappa_3 \mathbf{d}_3, \tag{5.c}$$

where $(\,)'$ and $\dot{(\,)}$ stand, respectively, for arclength and time derivatives; ξ is the (constant) mass per unit volume of the rod and $\mathcal{A}$ the cross sectional area; the quantities I_1 and I_2 are the principal moments of inertia of the cross section, E is Young's modulus, μ is the shear modulus, and J depends on the cross section shape. In the particular case of a circular cross section of radius R, one has $I_1 = I_2 = J/2 = \pi R^4/4$. The products EI_1 and EI_2 are the *principal bending stiffnesses* of the rod, and μJ is the *torsional stiffness*. The tangential component of the force, $\mathbf{d}_3 \cdot \mathbf{F}$, is the *tension* along the rod.

The coupled equations (5) constitute the dynamical Kirchhoff equations. These are three vector equations involving the local basis $(\mathbf{d}_1, \mathbf{d}_2, \mathbf{d}_3)$ and its derivatives, the force $\mathbf{F}$ and the torque $\mathbf{M}$, which total nine degrees of freedom; hence, the system is closed.

We can further simplify the Kirchhoff model by choosing the following length, time, and mass scales as measuring units:

$$[L] = \sqrt{\frac{I_1}{\mathcal{A}}}, \qquad [T] = \sqrt{\frac{\xi I_1}{E\mathcal{A}}}, \qquad [M] = \xi\sqrt{\mathcal{A}I_1}, \tag{6}$$

which amounts to make the replacements

$$\frac{\partial}{\partial s} \to \sqrt{\frac{\mathcal{A}}{I_1}}\frac{\partial}{\partial s}, \qquad \kappa \to \sqrt{\frac{\mathcal{A}}{I_1}}\kappa, \qquad \frac{\partial^2}{\partial t^2} \to \frac{E\mathcal{A}}{\xi I_1}\frac{\partial^2}{\partial t^2}, \tag{7.a}$$

$$\mathbf{F} \to E\mathcal{A}\,\mathbf{F}, \qquad \mathbf{M} \to E\sqrt{\mathcal{A}I_1}\mathbf{M}. \tag{7.b}$$

The Kirchhoff equations then reduce to the dimensionless form

$$\mathbf{F}'' = \ddot{\mathbf{d}}_3, \tag{8.a}$$

$$\mathbf{M}' + \mathbf{d}_3 \times \mathbf{F} = a\,\mathbf{d}_1 \times \ddot{\mathbf{d}}_1 + \mathbf{d}_2 \times \ddot{\mathbf{d}}_2, \tag{8.b}$$

$$\mathbf{M} = \kappa_1\mathbf{d}_1 + a\kappa_2\mathbf{d}_2 + b\kappa_3\mathbf{d}_3, \tag{8.c}$$

with

$$a \equiv \frac{I_2}{I_1}, \qquad b \equiv \frac{\mu J}{EI_1} \equiv \frac{J}{2I_1(1+\sigma)}, \tag{9}$$

where σ denotes the Poisson ratio, which ranges from 0, corresponding to hyperelasticity (if there is no striction as the material is stretched) to 1/2, corresponding to incompressible media (if the volume is unchanged as the material is stretched) [24]. The constant a measures the asymmetry of the cross section. Our convention is to orient the vector fields $\mathbf{d}_1$ and $\mathbf{d}_2$ such that I_1 and I_2 are, respectively, the larger and smaller bending stiffnesses. In this case, we have

$$0 < a \leq 1, \tag{10}$$

the value 1 being reached in the dynamically symmetric case where the moments of inertia are identical. The constant b is the *scaled torsional stiffness*. In the particular case of a circular cross section, one has

$$b = \frac{1}{1+\sigma} \in \left[\frac{2}{3}, 1\right]. \tag{11}$$

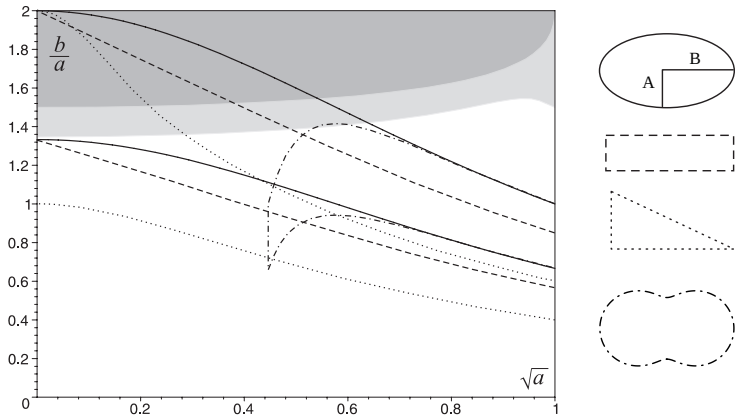

Fig. 1. The domains covered in (a, b) space by various cross section shapes are enclosed in black lines (solid = ellipses, dash = rectangles, dot = isosceles triangles, dash-dot = elliptic limaçons). The shades of gray pertain to the topics discussed in Sections 3 (where two bifurcation regimes are distinguished) and 5 (where the constant μ is introduced). Dark gray = tapelike regime with $\mu < 1$, light gray = thick regime with $\mu < 1$, white = thick regime with $\mu > 1$. The functions of a and b appearing as diagram coordinates are chosen so as to provide a realistic visual representation of the relative importance of each region.

Within the framework of linear elasticity theory [24], [26], [36], it is possible to compute the parameters a and b for a given cross section shape. For instance, if we consider elliptic cross sections with semi-axes A and B ($A < B$), we have

$$a = \frac{A^2}{B^2}, \qquad b = \frac{1}{1+\sigma}\,\frac{2a}{1+a}. \tag{12}$$

Extensive computations of torsional and bending stiffness for various shapes have been compiled in the classical engineering literature. The cases of elliptic-, rectangular-, and elliptic-limaçon-shaped cross sections are treated in [36]. In general, rods with cross sections made up of assembled flat pieces, like X or H shapes, have low torsional stiffnesses (small b). In addition, we computed approximate values for isosceles-triangular cross sections. Rather than giving the cumbersome formula for a and b in terms of the free parameters, we represent, in Figure 1, the domain covered in the (a, b) space for each of these particular shapes for realistic Poisson ratio (that is, for σ varying between 0 and 1/2). More data can be found, for example, in [32].

3. Equilibrium and Stability of Strips

In this section we consider the helical, circular, and straight static solutions of the Kirchhoff equations for strips. We first show that the class of equilibrium helical shapes is more restricted in the generic case $a \neq 1$ than in the case of symmetric cross sections. Indeed,

this result, as well as the ones described in Sections 4 and 5, show that the symmetric case is highly degenerate and that the behavior of strips is richer.

Experimental, analytical, and numerical results for static strips have been obtained recently by Champneys, Thompson, and van der Heijden [6], [7], [38], [39], [40]. In [6], they present a linear analysis of the static Kirchhoff equations for a straight strip and investigate numerically the existence of localizing buckling modes. This analysis is completed by a normal form analysis in [40] where it is shown that infinite rods have a tendency to localize after the bifurcation. Here, we will be able to obtain additional insights into the behavior of solutions close to the straight state through an amplitude equation analysis of the full, dynamical Kirchhoff equations valid for finite and infinite rods under a variety of boundary conditions. We first develop, in Section 3.2, a general perturbation scheme for the dynamical Kirchhoff equations near a given reference state; and then, in Section 3.3, perform a dynamical stability analysis for the straight strip by linearizing the Kirchhoff equations around the straight solution, recovering the results of Champneys and Thompson in the static case along the way. These results provide the necessary background for the amplitude equation analysis described in Section 4.

3.1. Simple Equilibrium Solutions

In order to investigate the existence of equilibrium solutions to the Kirchhoff equations for strips, we consider the static form of system (8). To do so, we integrate (8.a) once with respect to arclength, introduce the components of the force in the local basis $\mathbf{F} = F_1\mathbf{d}_1 + F_2\mathbf{d}_2 + F_3\mathbf{d}_3$, and project (8) along this basis to obtain a system of six equations involving the six unknowns F_1, F_2, F_3, κ_1, κ_2, and κ_3:

$$F_1' + \kappa_2 F_3 - \kappa_3 F_2 = 0, \tag{13.a}$$
$$F_2' + \kappa_3 F_1 - \kappa_1 F_3 = 0, \tag{13.b}$$
$$F_3' + \kappa_1 F_2 - \kappa_2 F_1 = 0, \tag{13.c}$$
$$\kappa_1' + (b-a)\,\kappa_2\kappa_3 - F_2 = 0, \tag{13.d}$$
$$a\,\kappa_2' + (1-b)\,\kappa_1\kappa_3 + F_1 = 0, \tag{13.e}$$
$$b\,\kappa_3' + (a-1)\,\kappa_1\kappa_2 = 0. \tag{13.f}$$

If $a = 1$, we see from (13.f) that the twist density κ_3 is constant.

The trivial equilibrium solutions of these equations are straight strips, for which $\kappa_1 = \kappa_2 = 0$. Inserting this into (13) leads to a general solution of the form

$$\kappa = \kappa_3\mathbf{d}_3, \qquad \mathbf{F} = F_3\mathbf{d}_3, \tag{14}$$

where $\mathbf{d}_3$ has a constant orientation along the arclength, and κ_3 and F_3 are arbitrary constants. Hence, for given a and b, the straight strips constitute a two-parameter family of solutions, characterized by a twist density κ_3 and tension F_3.

Helical solutions are obtained by assuming constant Frenet curvature κ and torsion τ, and using expressions (4) for the twist vector. We now show, by contradiction, that the only possible helical strips are Frenet strips, that is, strips with zero internal twist. Notice that, unlike the case $a = 1$, we cannot assume *a priori* that the twist density

κ_3 is constant. Hence, we take ζ in (4) to be an arbitrary function of s. Equations (13) expressed in terms of ζ read:

$$F_1' - (\zeta' + \tau)F_2 + \kappa F_3 \cos\zeta = 0, \tag{15.a}$$
$$F_2' + (\zeta' + \tau)F_1 - \kappa F_3 \sin\zeta = 0, \tag{15.b}$$
$$F_3' + \kappa F_2 \sin\zeta - \kappa F_1 \cos\zeta = 0, \tag{15.c}$$
$$F_2 = \kappa \left[(b + 1 - a)\zeta' + (b - a)\tau\right] \cos\zeta, \tag{15.d}$$
$$F_1 = \kappa \left[(b + a - 1)\zeta' + (b - 1)\tau\right] \sin\zeta, \tag{15.e}$$
$$b\,\zeta'' = (1 - a)\,\kappa^2 \sin\zeta \cos\zeta. \tag{15.f}$$

We now prove that ζ is constant along the strip and is actually an integer multiple of $\pi/2$. Consider the following linear combination of (15.a) and (15.b):

$$\begin{aligned}&\left[F_1' - (\zeta' + \tau)F_2 + \kappa F_3 \cos\zeta\right] \sin\zeta \\ &\quad + \left[F_2' + (\zeta' + \tau)F_1 - \kappa F_3 \sin\zeta\right] \cos\zeta = 0,\end{aligned} \tag{16}$$

which reduces to

$$F_1' \sin\zeta + F_2' \cos\zeta + (\zeta' + \tau)(F_1 \cos\zeta - F_2 \sin\zeta) = 0. \tag{17}$$

Substituting (15.d) and (15.e) into (17) yields (provided $\kappa \neq 0$)

$$[4b + 2(1 - a)\cos 2\zeta]\,\zeta'' - (1 - a)(2\zeta' + \tau)^2 \sin 2\zeta = 0. \tag{18}$$

We can substitute the expression for ζ'' from (15.f) into (18) to obtain

$$(1 - a)\kappa^2 \sin 4\zeta + 2b[2\kappa^2 - 4\zeta'^2 - 4\tau\zeta' - \tau^2] \sin 2\zeta = 0. \tag{19}$$

Assuming $\zeta' \neq 0$ for s lying in some interval, we multiply both sides of (15.f) by ζ' and integrate this equation once:

$$b\zeta'^2 = (1 - a)\,\kappa^2 \sin^2\zeta + C = \frac{(1 - a)\kappa^2}{2}(1 - \cos 2\zeta) + C, \tag{20}$$

where C is an integration constant. We can eliminate ζ'^2 between (19) and (20):

$$4b\tau\zeta' = 3(1 - a)\kappa^2 \cos 2\zeta + 2(b + a - 1)\kappa^2 - 4C - b\tau^2. \tag{21}$$

Squaring both sides of (21) and eliminating ζ'^2 by using (20) yields

$$\begin{aligned}&8b\tau^2[(1 - a)\kappa^2(1 - \cos 2\zeta) + 2C] \\ &\quad - [3(1 - a)\kappa^2 \cos 2\zeta + 2(b + a - 1)\kappa^2 - 4C - b\tau^2]^2 = 0.\end{aligned} \tag{22}$$

Since ζ is assumed not constant, the coefficient of every power of $\cos 2\zeta$ must vanish independently in equation (22). However, the coefficient of $\cos^2 2\zeta$, namely $-9(1-a)^2\kappa^4$, is negative for any nonvanishing value of the curvature, contradicting our assumption that ζ varies with s. Returning to (15.f) and setting $\zeta'' = 0$, we see that

$$\zeta = n\frac{\pi}{2}, \qquad n \in \mathbb{Z}. \tag{23}$$

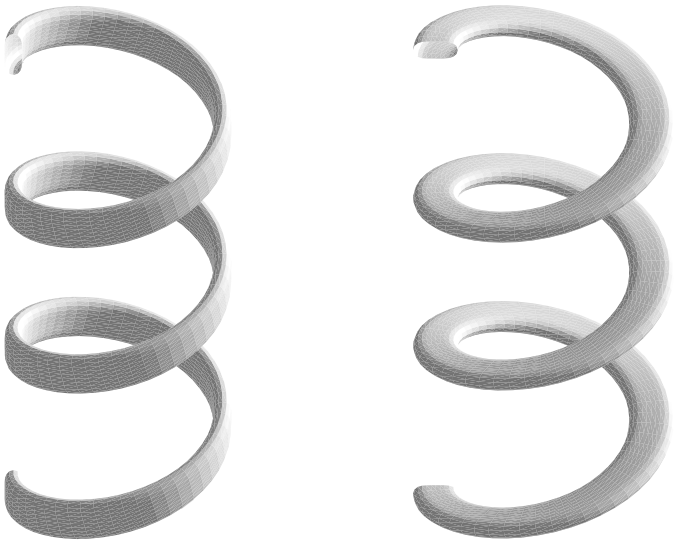

Fig. 2. A binormal helix (left) and a normal helix (right).

We can now solve the system (15). For given κ and τ, two solutions arise, depending only on the parity of n. The helices and rings corresponding to even n are referred to as *binormal helices* and *binormal rings*, since the direction of highest bending stiffness ($\mathbf{d}_2$) lies along the binormal. If we further require that the rings must be closed on themselves, the boundary conditions impose $n/2$ to be an integer. The helices and rings corresponding to odd values of n are named *normal helices* and *normal rings*, since the direction of highest bending stiffness lies along the normal. Both types of helices, represented in Figure 2, are *Frenet helices*. In the binormal case, we have

$$\kappa = \kappa \mathbf{d}_2 + \tau \mathbf{d}_3, \qquad \mathbf{F} = (b-a)\tau\kappa, \tag{24}$$

whereas in the normal case, the solution is

$$\kappa = \kappa \mathbf{d}_1 + \tau \mathbf{d}_3, \qquad \mathbf{F} = (b-1)\tau\kappa. \tag{25}$$

For fixed $a \neq 1$ and b, the helical and ringlike strips together form a two-parameter family, characterized by a Frenet curvature κ and a Frenet torsion τ in contrast to the degenerate case $a = 1$, where there exists a three-parameter family of helical solutions, characterized by curvature, torsion, and an arbitrary constant twist density.

3.2. Perturbation Scheme

If an exact solution of the Kirchhoff equations (8) is known, perturbed states of the system in a small neighborhood of this reference solution can be systematically studied by expanding the relevant variables as power series in a small parameter ε characterizing the distance from the (unperturbed) reference state. To do so, we introduce a near-identity

rotation matrix **B** mapping the unperturbed local basis onto the perturbed basis:

$$\left(\begin{array}{ccc} \mathbf{d}_1 & \mathbf{d}_2 & \mathbf{d}_3 \end{array} \right) \equiv \left(\begin{array}{ccc} \mathbf{d}_1^{(0)} & \mathbf{d}_2^{(0)} & \mathbf{d}_3^{(0)} \end{array} \right) \mathbf{B}. \tag{26}$$

We now expand the entries of **B** as series of ε. The simplest form of the expansion is

$$\mathbf{B} \equiv \mathbf{1} + \varepsilon\, \mathbf{A}^{(1)} + \varepsilon^2 \left(\mathbf{A}^{(2)} + \mathbf{S}^{(2)}\right) + \varepsilon^3 \left(\mathbf{A}^{(3)} + \mathbf{S}^{(3)}\right) + \cdots, \tag{27}$$

where **1** is the identity matrix and the $\mathbf{A}^{(k)}$'s are general antisymmetric matrices,

$$\mathbf{A}^{(k)} \equiv \begin{pmatrix} 0 & -\alpha_3^{(k)} & \alpha_2^{(k)} \\ \alpha_3^{(k)} & 0 & -\alpha_1^{(k)} \\ -\alpha_2^{(k)} & \alpha_1^{(k)} & 0 \end{pmatrix}. \tag{28}$$

The matrices $\mathbf{S}^{(k)}$ are symmetric and are found to depend only on the entries of $\mathbf{A}^{(1)}$ to $\mathbf{A}^{(k-1)}$. Our goal is to obtain expressions for the entries of the twist matrix **K** and the spin matrix **W** in terms of the perturbed variables. Using definitions (1.a) and (26), we have

$$\frac{\partial}{\partial s} \left[\left(\begin{array}{ccc} \mathbf{d}_1^{(0)} & \mathbf{d}_2^{(0)} & \mathbf{d}_3^{(0)} \end{array} \right) \mathbf{B} \right] = \left(\begin{array}{ccc} \mathbf{d}_1^{(0)} & \mathbf{d}_2^{(0)} & \mathbf{d}_3^{(0)} \end{array} \right) \mathbf{B}\, \mathbf{K}, \tag{29}$$

which can be reexpressed as

$$\left(\begin{array}{ccc} \mathbf{d}_1^{(0)} & \mathbf{d}_2^{(0)} & \mathbf{d}_3^{(0)} \end{array} \right) \left[\mathbf{K}^{(0)}\, \mathbf{B} - \mathbf{B}\, \mathbf{K} + \frac{\partial \mathbf{B}}{\partial s} \right] = \mathbf{0}. \tag{30}$$

Since the basis vectors are independent and the matrix **B** is orthogonal, (30) yields

$$\mathbf{K} = \mathbf{B}^{\top} \left(\mathbf{K}^{(0)}\, \mathbf{B} + \frac{\partial \mathbf{B}}{\partial s} \right). \tag{31}$$

Analogous expressions hold for the spin vector ω. We are now able to write down the Kirchhoff equations (8) to order k, for any given unperturbed state, in terms of the six variables

$$\mathbf{X}^{(k)} \equiv \left(F_1^{(k)}, F_2^{(k)}, F_3^{(k)}, \alpha_1^{(k)}, \alpha_2^{(k)}, \alpha_3^{(k)} \right). \tag{32}$$

3.3. Stability Analysis for the Straight Rod

3.3.1. Dispersion Relation. The stability analysis is performed by linearizing the Kirchhoff equations around the static straight solution. This is achieved by substituting the expansions for the force, twist, and spin vectors, truncated to first order, into the system (8), taking (14) as expressions for the unperturbed variables $\mathbf{F}^{(0)}$ and $\kappa^{(0)}$, and setting $\omega^{(0)} = \mathbf{0}$. This yields, in matrix form,

$$\mathbf{L}\, \mathbf{X}^{(1)} = \mathbf{0}, \tag{33}$$

where the linear operator $\mathbf{L}$ takes the form

$$\mathbf{L} \equiv \begin{pmatrix} \frac{\partial^2}{\partial s^2} - \gamma^2 - 2\gamma\frac{\partial}{\partial s} & 0 & 2\rho\gamma^3\frac{\partial}{\partial s} & \rho\gamma^2\frac{\partial^2}{\partial s^2} - \rho\gamma^4 - \frac{\partial^2}{\partial t^2} & 0 \\ 2\gamma\frac{\partial}{\partial s} & \frac{\partial^2}{\partial s^2} - \gamma^2 & 0 & \rho\gamma^4 - \rho\gamma^2\frac{\partial^2}{\partial s^2} + \frac{\partial^2}{\partial t^2} & 2\rho\gamma^3\frac{\partial}{\partial s} & 0 \\ 0 & 0 & \frac{\partial^2}{\partial s^2} & 0 & 0 & 0 \\ 0 & -1 & 0 & (b-a)\gamma^2 + \frac{\partial^2}{\partial s^2} - \frac{\partial^2}{\partial t^2} & (b-a-1)\gamma\frac{\partial}{\partial s} & 0 \\ 1 & 0 & 0 & (1+a-b)\gamma\frac{\partial}{\partial s} & (b-1)\gamma^2 + a\left(\frac{\partial^2}{\partial s^2} - \frac{\partial^2}{\partial t^2}\right) & 0 \\ 0 & 0 & 0 & 0 & 0 & b\frac{\partial^2}{\partial s^2} - (1+a)\frac{\partial^2}{\partial t^2} \end{pmatrix}. \tag{34}$$

The constants γ and ρ are defined as

$$\gamma \equiv \kappa_3^{(0)}, \qquad \rho \equiv \frac{F_3^{(0)}}{(\kappa_3^{(0)})^2}. \tag{35}$$

For ρ to be well-defined, we limit our analysis to strips with nonzero twist. The parameter γ represents the twist density of the initial state (the twisted straight rod). The dimensionless parameter ρ controls the critical value of the physical parameter where buckling occurs. For a rod with circular cross sections, the Euler-Love-Timoshenko buckling occurs for $\rho < b^2/4$. Buckling can occur either by a decrease in tension $F_3^{(0)}$ with constant twist, by an increase in the twist density $\kappa_3^{(0)}$ with constant tension, or, in general, by decreasing the parameter ρ past a critical value. Next, we look for the fundamental solutions, or *normal modes*, of (33),

$$\mathbf{X}^{(1)} = A\,\mathbf{u}\exp\gamma(\sigma t + ins), \tag{36}$$

where A is a constant complex amplitude, $\mathbf{u}$ is a constant vector with a fixed norm, σ is a complex constant, and n is a real constant. The factor γ in the exponential has been introduced for convenience. In the following, n is called the *spatial frequency* (although, strictly speaking, this name would more appropriately refer to $n\gamma$) and, similarly, σ is called the *growth exponent*. Inserting (36) into (33) yields

$$\mathbf{M}\,\mathbf{u} = 0, \tag{37}$$

where $\mathbf{M}$ is a matrix involving σ and n:

$$\mathbf{M} \equiv \begin{pmatrix} -(1+n^2)\gamma^2 & -2in\gamma^2 & 0 & 2in\rho\gamma^4 & -(1+n^2)\rho\gamma^4 - \sigma^2\gamma^2 & 0 \\ 2in\gamma^2 & -(1+n^2)\gamma^2 & 0 & (1+n^2)\rho\gamma^4 + \sigma^2\gamma^2 & 2in\rho\gamma^4 & 0 \\ 0 & 0 & -n^2\gamma^2 & 0 & 0 & 0 \\ 0 & -1 & 0 & (b-a-n^2-\sigma^2)\gamma^2 & i(b-a-1)n\gamma^2 & 0 \\ 1 & 0 & 0 & i(1+a-b)n\gamma^2 & (b-1-an^2-a\sigma^2)\gamma^2 & 0 \\ 0 & 0 & 0 & 0 & 0 & [-bn^2-(1+a)\sigma^2]\gamma^2 \end{pmatrix}. \tag{38}$$

There exist nontrivial solutions for $\mathbf{u}$ only if $\det\mathbf{M} = 0$. This condition yields the *dispersion relation*,

$$n^2\ \left(\ (1+a)\,\sigma^2 + bn^2\ \right)\ \left(\ \left\{a\,(n^2-1)^2 + (1+a)\gamma^{-2}\,(n^2+1) + \ \gamma^{-4}\right\}\ \sigma^4\right.$$

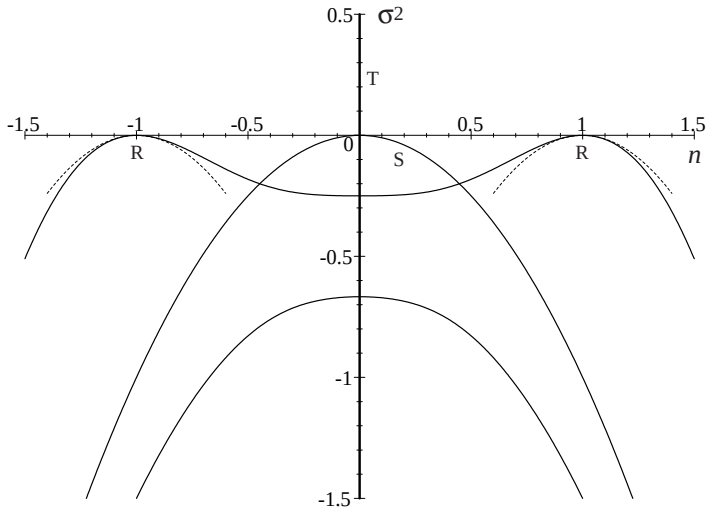

Fig. 3. The dispersion relation for $a = 1/2$, $b = 3/2$, $\rho = 3/2$, $\gamma = 1$. The straight strip is stable for these values of the parameters (the pathological exponentially growing T modes that lie on the vertical axis are not considered to be unstable; see text).

$$
\begin{aligned}
&+\left\{2a\,n^6+[(1+a)(\rho-b)+1-4a+a^2+(1+a)\gamma^{-2}]\,n^4\right.\\
&+[2(1+a)(b-\rho)-2(1-a+a^2)+2(\rho+3(1+a-b))\gamma^{-2}]\,n^2\\
&\left.+(1+a)(\rho-b)+1+a^2+[2(\rho-b)+1+a]\gamma^{-2}\right\}\,\sigma^2\\
&+(1-n^2)^2\,\left\{a\,n^4+[(1+a)(b+\rho)-b^2-2a]\,n^2\right.\\
&+\left.\ (\rho+1-b)(\rho+a-b)\}\ \right)=0. \qquad (39)
\end{aligned}
$$

The stability of the straight strip with given values of the parameters a, b, γ, and ρ can be studied by analyzing the dispersion relation. Modes that grow exponentially in time, characterized by $\mathrm{Re}(\sigma) > 0$, correspond to the *unstable modes*. Since the dispersion relation is an equation in σ^2, its roots come in pairs with opposite signs—hence the straight rod becomes linearly unstable if the dispersion relation allows for normal modes with positive or nonreal values of σ^2. Exceptions to this rule are the modes with $n = 0$ and arbitrary σ corresponding to the factor n^2 in (39). We now make the assumption that nonreal values of σ^2 are not allowed by the dispersion relation. This is confirmed for a wide range of values of the system parameters, and is readily established for certain fixed spatial frequencies, independently of the values of the parameters.

In order to determine the region where unstable modes are allowed, we must investigate the conditions for the existence of *neutral modes* characterized by $\sigma = 0$. Before doing this, we first examine and identify various sets of solutions of the dispersion relation.

The dispersion relation is displayed in Figure 3 for particular values of the parameters for which the straight rod is stable. The left-hand side of (39) is a product of three factors, each one vanishing on a different branch, or set of branches, of the dispersion relation. In

the following, the branch associated with the first factor, n^2, is referred to as the *T branch*, because the corresponding normal *T modes* describe variations in *tension* in the course of time. The branch associated with the second factor, $(1+a)\,\sigma^2 + bn^2$, is referred to as the *S branch*, because among the corresponding normal *S modes*, there is a neutral mode representing a *self-rotation* of the strip around its centerline. The third factor, referred to as the *R branch*, is associated with nonaxisymmetric rotation of the filament.

The null space of the operator $\mathbf{L}$ for a given solution of the dispersion relation is determined by solving the equation (37) for the corresponding values of σ and n. On the T and S branches, the normalized solutions $\mathbf{u}$ are given by $\mathbf{u}_\mathrm{T}$ and $\mathbf{u}_\mathrm{S}$, where

$$\mathbf{u}_\mathrm{T} \equiv (0,\,0,\,1,\,0,\,0,\,0)\,, \tag{40.a}$$

$$\mathbf{u}_\mathrm{S} \equiv (0,\,0,\,0,\,0,\,0,\,1)\,. \tag{40.b}$$

The T modes. The T branch corresponds to fundamental solutions of the linearized Kirchhoff equations of the form,

$$\mathbf{F} = (\rho\gamma^2 + \varepsilon\; A_\mathrm{T} \exp\gamma\sigma t)\;\mathbf{d}_3, \quad \kappa = \gamma\;\mathbf{d}_3, \quad \omega = \mathbf{0}, \tag{41}$$

where A_T and σ are arbitrary complex constants. These modes are such that the strip remains straight and is subject to an applied longitudinal tension either oscillating in time with an arbitrary frequency, or growing in time exponentially. The exponentially growing modes, being present in the whole parameter space, do not actually correspond to an instability, but reflect instead the arbitrariness of the time dependence of the tensile constraints that can be applied to the rod. The static T mode ($\sigma = 0$) corresponds to a constant deviation in tension from the unperturbed configuration, which can be taken into account by redefining ρ.

The S modes. Taking into account the expressions (31) for the components of the twist vector, and setting

$$c_\mathrm{S}^2 \equiv \frac{b}{1+a}, \tag{42}$$

the S branch is seen to correspond to the following real fundamental solutions:

$$\mathbf{F} = \rho\gamma^2\;\mathbf{d}_3, \tag{43.a}$$

$$\kappa = \left\{\gamma + \varepsilon\; n\gamma\left[i A_\mathrm{S} \exp in\gamma\;(s \pm c_\mathrm{S}\,t) + \text{c.c.}\right]\right\}\;\mathbf{d}_3, \tag{43.b}$$

$$\omega = \pm\,\varepsilon\; n\gamma c_\mathrm{S}\left[i A_\mathrm{S} \exp in\gamma(s \pm c_\mathrm{S}\,t) + \text{c.c.}\right]\;\mathbf{d}_3, \tag{43.c}$$

where A_S is an arbitrary real amplitude, n is an arbitrary real frequency, and "c.c." indicates the complex conjugate of the preceding term. For $n \neq 0$, these are the well-known linear *twist waves* (or *torsional waves* [24]) traveling along the straight rod at fixed velocity c_S. For $n = 0$, the near-identity matrix $\mathbf{B}$ takes the form

$$\mathbf{B} = \begin{pmatrix} 1 & -\varepsilon A_\mathrm{S} & 0 \\ \varepsilon A_\mathrm{S} & 1 & 0 \\ 0 & 0 & 1 \end{pmatrix}. \tag{44}$$

To first order, this represents a fixed global rotation of the straight rod around its centerline.

The R modes. We now consider the third factor of the dispersion relation (39). We see that $n^2 = 1$, $\sigma = 0$ satisfies the dispersion relation for all values of the parameters. Setting

$$\nu \equiv n \mp 1 \tag{45}$$

and keeping the terms of lowest degree in ν and σ in the dispersion relation yields

$$\sigma^2 = -\rho\gamma^2\nu^2 + \mathrm{o}(\nu^2), \tag{46}$$

which holds in a neighborhood of the points $n = \pm 1$, $\sigma = 0$. The asymptotic branches (46) are referred to in the following as the *R branches*, and the corresponding normal *R modes* describe, for $\sigma = 0$, a *rotation* of the straight rod around an axis different from its centerline. The R modes are unstable if $\rho < 0$, that is, if the rod is in a state of compression rather than extension. In an experiment where the rod is initially subject to a strong positive tension which is gradually decreased, these unstable R modes, which account for the tendency of the rod to bend under compression, do not show up as long as the tension remains positive. The solution $\mathbf{u}_\mathrm{R}$ of equation (37) for $n = 1$ and $\sigma = 0$ is

$$\mathbf{u}_\mathrm{R} \equiv (0, 0, 0, 1, i, 0)\,, \tag{47}$$

whereas the solution for $n = -1, \sigma = 0$ is the complex conjugate, $\mathbf{u}_\mathrm{R}^*$. The corresponding real solutions (static R modes) take the form

$$\mathbf{F} = \rho\gamma^2\,\mathbf{d}_3, \tag{48.a}$$

$$\alpha_1^{(1)} = A_\mathrm{R} \exp i\gamma s + \text{c.c.}, \tag{48.b}$$

$$\alpha_2^{(1)} = i A_\mathrm{R} \exp i\gamma s + \text{c.c.}, \tag{48.c}$$

$$\alpha_3^{(1)} = 0, \tag{48.d}$$

where A_R is an arbitrary complex amplitude. It is convenient to represent some of the quantities of interest in terms of the spatially fixed coordinate triad $(\mathbf{e}_\mathrm{X}, \mathbf{e}_\mathrm{Y}, \mathbf{e}_\mathrm{Z})$. Choosing $\mathbf{d}_3^{(0)}$ to point along $\mathbf{e}_\mathrm{Z}$, the unperturbed basis $(\mathbf{d}_1^{(0)}, \mathbf{d}_2^{(0)}, \mathbf{d}_3^{(0)})$ is represented as

$$\begin{pmatrix} \mathbf{d}_1^{(0)} & \mathbf{d}_2^{(0)} & \mathbf{d}_3^{(0)} \end{pmatrix} = \begin{pmatrix} \mathbf{e}_\mathrm{X} & \mathbf{e}_\mathrm{Y} & \mathbf{e}_\mathrm{Z} \end{pmatrix} \begin{pmatrix} \cos\gamma s & -\sin\gamma s & 0 \\ \sin\gamma s & \cos\gamma s & 0 \\ 0 & 0 & 1 \end{pmatrix}. \tag{49}$$

It is now possible, using (26), to express the perturbed tangent vector $\mathbf{d}_3$ in the form

$$\mathbf{d}_3 = \mathbf{e}_\mathrm{Z} - 2\varepsilon\,(\mathrm{Im}A_\mathrm{R}\,\mathbf{e}_\mathrm{X} + \mathrm{Re}A_\mathrm{R}\,\mathbf{e}_\mathrm{Y}). \tag{50}$$

Comparing $\mathbf{d}_3$ with the unperturbed tangent vector $\mathbf{d}_3^{(0)} = \mathbf{e}_\mathrm{Z}$, one sees that (50) represents, to first order, a fixed global rotation around an axis distinct from the unperturbed centerline.

We now examine the nonstatic R modes, corresponding to small $|\nu| \neq 0$ in equation (46). Assuming that the corresponding solutions $\mathbf{u}$ of equation (37) do not differ much from $\mathbf{u}_\mathrm{R}$ and $\mathbf{u}_\mathrm{R}^*$, and using (46), we obtain real solutions of the form

$$\mathbf{F} \simeq \rho\gamma^2\,\mathbf{d}_3, \tag{51.a}$$

$$\alpha_1^{(0)} \simeq A_\mathrm{R} \exp i\gamma[\nu(s \pm c_\mathrm{R}t) + s] + \text{c.c.}, \tag{51.b}$$

$$\alpha_2^{(0)} \simeq i A_\mathrm{R} \exp i\gamma[\nu(s \pm c_\mathrm{R}t) + s] + \text{c.c.}, \tag{51.c}$$

$$\alpha_3^{(0)} \simeq 0, \tag{51.d}$$

where A_R is a complex amplitude, ν is a small real constant, and

$$c_R^2 \equiv \rho\gamma^2 \equiv F_3^{(0)}. \tag{52}$$

Taking the sum and the difference of two solutions of type (51) with opposite values of ν and complex conjugate values of A_R, and computing for both combinations the corresponding tangent vector $\mathbf{d}_3$, we obtain two different types of wave propagation along the two axes:

$$(1) \quad \mathbf{d}_3 = \mathbf{e}_Z + 2\varepsilon\ (\mathrm{i}A_R \exp \mathrm{i}\gamma\nu(s \pm c_R t) + \mathrm{c.c.})\ \mathbf{e}_X, \tag{53.a}$$

$$(2) \quad \mathbf{d}_3 = \mathbf{e}_Z - 2\varepsilon\ (A_R \exp \mathrm{i}\gamma\nu(s \pm c_R t) + \mathrm{c.c.})\ \mathbf{e}_Y. \tag{53.b}$$

These expressions describe the familiar plane waves propagating in rods under tension with a velocity proportional to the square root of the tension [24]. In twisted strips, these plane waves appear only at low frequencies (small $|\nu|$).

A typical plot of the dispersion relation is shown in Figure 3, and the previously discussed T, S, and R branches are indicated.

3.3.2. Unstable Modes and Critical Point. The neutral modes described earlier (the static T, S, and R modes) exist everywhere in parameter space. Their existence is not an indication that the rod is unstable but merely a consequence of particular symmetries of the equations. We now look for the remaining neutral modes by setting $\sigma = 0$ in the dispersion relation. As σ vanishes, the third factor of the dispersion relation (39) equated to zero reads

$$a\, n^4 + [(1+a)(b+\rho) - b^2 - 2a]\, n^2 + (\rho + 1 - b)(\rho + a - b) = 0. \tag{54}$$

This equation does not involve γ. In order for neutral modes to exist, (54) must admit real solutions[2] for n, or positive solutions for n^2. The position of the roots in the complex plane can be determined by considering the conditions for the discriminant Δ, the sum of the squared roots Σ, and the product of the squared roots Π, to vanish:

$$\Delta \equiv [(1+a)(b+\rho) - b^2 - 2a]^2 - 4a(\rho + 1 - b)(\rho + a - b) = 0, \tag{55.a}$$

$$\Sigma \equiv 2 + \frac{b^2 - (1+a)(b+\rho)}{a} = 0, \tag{55.b}$$

$$\Pi \equiv \frac{(\rho + 1 - b)(\rho + a - b)}{a} = 0. \tag{55.c}$$

[2] Actually, solutions with imaginary n exist in some cases and are acceptable as well: They describe deformations proportional to hyperbolic functions of the arclength ($\sinh\gamma\,|n|\,s$ and $\cosh\gamma\,|n|\,s$). They are meaningful only if finite-length strips are considered. If the strip is long enough, or if γ is large, they are (with an appropriate normalization factor) exponentially small everywhere along the strip except in a close neighborhood of the strip ends, so that they introduce boundary layers. As such, they are not involved in the large-scale geometry of the strip and may be ignored for the purpose of the nonlinear analysis of Section 4. In Section 5, we treat specifically finite-length problems. Nevertheless, we compute only dominant-order solutions, in which the hyperbolic modes may be shown to play no role. Therefore, they are dropped from the discussion for the remainder of the paper.

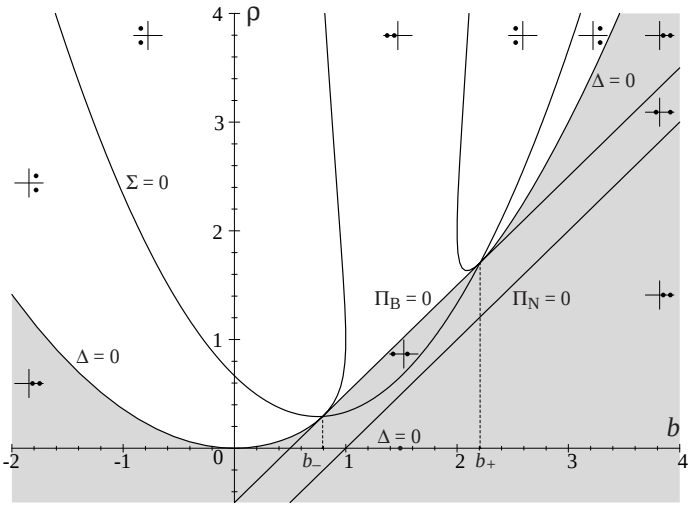

Fig. 4. Stability diagram for $a = 1/2$, with b extending beyond physical range. The small frames concern the regions between the curves in the (b, ρ) plane and show the locations in the complex plane of the two solutions for n^2, with positive real axis pointing right and positive imaginary axis pointing up. The isolated point on the axis $\rho = 0$ is part of the curve $\Delta = 0$. The gray zone is the region of instability.

The last relation factors to

$$\Pi_N \equiv \rho + 1 - b = 0, \tag{56.a}$$

$$\Pi_B \equiv \rho + a - b = 0, \tag{56.b}$$

which are exactly the conditions for the strip to be a normal helix or a binormal helix, respectively, in the limit of vanishing curvature: see (35) and (24)–(25).

For fixed $a \neq 1$, the curve $\Delta = 0$, the parabola $\Sigma = 0$, and the straight line $\Pi_B = 0$ are found to meet at exactly two points (b_-, ρ_-) and (b_+, ρ_+) in the (b, ρ) plane, with

$$b_\pm \equiv 1 + a \pm \sqrt{1-a}, \tag{57.a}$$

$$\rho_\pm \equiv 1 \pm \sqrt{1-a}. \tag{57.b}$$

Figure 4 depicts the situation for $a = 1/2$, which is a typical case in the sense that any value of a other than 1 leads to the same qualitative layout of the curves. This diagram is equivalent to Figure 1(a) in Champneys and Thompson (1996) [6]. See Table 1 for a translation of Champneys and Thompson's notations into our notations. Since equation (54) does not depend on γ, ρ is the only relevant parameter that can be adjusted in the course of an experiment and is accordingly referred to as the *control parameter*. High values of ρ correspond to conditions of strong tension, and in this regime, the straight strip is stable, that is, $\sigma^2 < 0$ for any real n, or positive n^2. As ρ decreases from the region of stability, it eventually reaches a critical value ρ_C for which the first neutral mode, which we will refer to as the *neutral C mode*, shows up and, beyond this critical point,

Table 1. Correspondence between our notations and Champneys, Thompson, and van der Heijden's notations. Their parameter ρ has been renamed $\tilde{\rho}$ in order to distinguish it from our ρ. Also, their definition of ν differs from one paper to another so that the original symbol ν in the table pertains to [6], [7], [39], whereas the symbol $\tilde{\nu}$ pertains to [40].

Our Notations	**van der Heijden et al. Notations**
$a = \min\left(1+\tilde{\rho}, \frac{1}{1+\tilde{\rho}}\right)$	$\tilde{\rho} = a - 1 \quad \text{or} \quad \tilde{\rho} = \frac{1}{a} - 1$
$b = \frac{\min(1+\tilde{\rho},1)}{1+\nu} = \frac{2\min(1+\tilde{\rho},1)}{(2+\tilde{\rho})(1+\tilde{\nu})}$	$\nu = \frac{a}{b} - 1 \quad \text{or} \quad \nu = \frac{1}{b} - 1$
$\rho = \frac{\min(1+\tilde{\rho},1)}{(1+\nu)^2 m^2} = \frac{4\min(1+\tilde{\rho},1)}{(2+\tilde{\rho})^2(1+\tilde{\nu})^2 m^2}$	$\tilde{\nu} = \frac{2a}{(1+a)b} - 1$
	$m = \frac{b}{\sqrt{a\rho}} \quad \text{or} \quad m = \frac{b}{\sqrt{\rho}}$

the dispersion relation admits solutions with real n and positive σ, which correspond to unstable modes. One sees from Figure 4 that, as ρ crosses the critical value, two qualitatively different situations arise, depending on the value of b. If b ranges between b_- and b_+, the first neutral mode appears with a spatial frequency $n_C = 0$, leading to a pitchfork bifurcation. If b lies outside this interval, two opposite critical frequencies $\pm n_C$ appear, each one being a double root of equation (54), leading to a Hamiltonian Hopf bifurcation. Note that, for $a \neq 1$, the line of normal helices $\Pi_N = 0$ is always located below the pitchfork line $\Pi_B = 0$, which proves, in the small-curvature limit, that the normal helices are unstable.

In the symmetric case ($a = 1$), the curve $\Delta = 0$ degenerates into a parabola and two identical vertical straight lines, while $\Pi = 0$ also corresponds to a pair of identical straight lines. There is no possibility of a zero-frequency bifurcation, except for the single value $b = 2$ (see Figure 5).

In the case of a flat elliptic cross section, that is, with a sufficiently small, the interval $[b_-, b_+]$ covers 3/4 of the physical range of b in the case of elliptic cross sections, with only the smaller values lying outside this interval, leading to a zero-frequency bifurcation for most of the physical values of b. This is visible in Figure 1, which shows the boundary $b = b_-$ in (a, b) space as the common edge of the two darkest shades of gray. Therefore, the pitchfork regime corresponds to flat cross sections with large enough torsional stiffness. In the following, this regime will be termed the *tapelike regime*, in compliance with the terminology of van der Heijden et al. [40], while the regime corresponding to $n_C \neq 0$ will be named the *thick regime*.

In the tapelike regime, the first instability appears as Π_B vanishes; hence, the straight rod becomes unstable due to the presence of nearby binormal helical strips. From equation (56.b), the critical value of ρ in the tapelike regime is

$$\rho_C^{TL} \equiv b - a. \tag{58}$$

In the thick regime, the first instability appears as the discriminant Δ vanishes. We now have to determine the critical values, ρ_C^{th}, of ρ, and the critical values $\pm n_C^{th}$ of the frequency ($+n_C^{th}$ denoting the positive one) in this case. For $a < 1$, ρ_C^{th} is the smallest

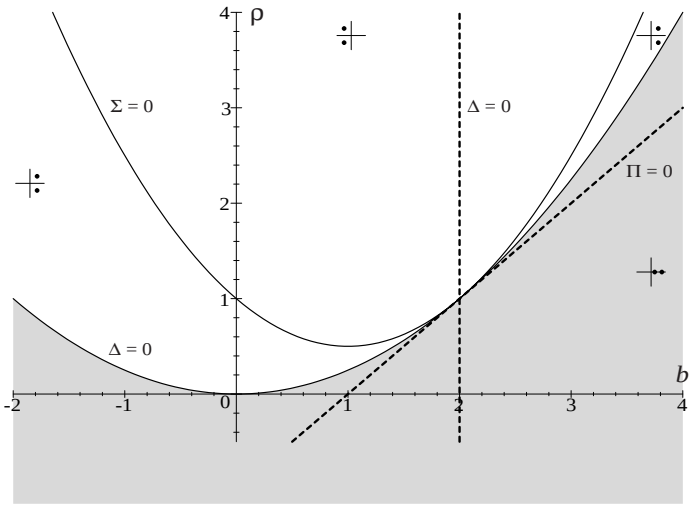

Fig. 5. Stability diagram for $a = 1$ (symmetric case). The small frames concern regions enclosed in solid lines and show the locations of the two solutions for n^2 in the complex plane, with positive real axis pointing right and positive imaginary axis pointing up. The gray zone is the region of instability. The tapelike (i.e., pitchfork) regime interval degenerates into a single point.

root of equation (55.a),

$$\rho_{\mathrm{C}}^{\mathrm{th}} \equiv \frac{(b-1-a)\left[b(1+a)-4a-2\sqrt{a\,(b-2)}\sqrt{b-2a}\right]}{(1-a)^2}. \tag{59}$$

The frequency $n_{\mathrm{C}}^{\mathrm{th}}$ is then given by the positive double root of (54):

$$n_{\mathrm{C}}^{\mathrm{th}} \equiv \sqrt{1+\frac{b^2-(1+a)(b+\rho_{\mathrm{C}}^{\mathrm{th}})}{2a}}. \tag{60}$$

Figures 6 and 7 show the solutions of the dispersion relation for slightly supercritical states of the rod in the tapelike and thick regimes, respectively.

For $a = 1$, realistic rods have $b \leq 1$ and only the thick regime values are relevant. In this case, one obtains the well-known Love criterion for twist instability [26],

$$\rho_{\mathrm{C}}^{a=1} \equiv \frac{b^2}{4}, \qquad n_{\mathrm{C}}^{a=1} \equiv \left|1-\frac{b}{2}\right|. \tag{61}$$

Having obtained the critical frequencies $n_{\mathrm{C}}^{\mathrm{TL}}$ and $n_{\mathrm{C}}^{\mathrm{th}}$, we must now determine the corresponding solutions $\mathbf{u}_{\mathrm{C}}^{\mathrm{TL}}$ and $\mathbf{u}_{\mathrm{C}}^{\mathrm{th}}$ of equation (37). We obtain for both regimes

$$\mathbf{u}_{\mathrm{C}} \equiv \left(-i\rho\gamma^2\chi,\, \rho\gamma^2,\, 0,\, 1,\, i\,\chi,\, 0\right), \tag{62}$$

where χ vanishes in the tapelike regime and $\chi = \chi^{\mathrm{th}}$ in the thick regime, with

$$\chi^{\mathrm{th}} \equiv \frac{\rho_{\mathrm{C}}^{\mathrm{th}}+a-b+(n_{\mathrm{C}}^{\mathrm{th}})^2}{n_{\mathrm{C}}^{\mathrm{th}}(a+1-b)} \equiv \frac{n_{\mathrm{C}}^{\mathrm{th}}(a+1-b)}{\rho_{\mathrm{C}}^{\mathrm{th}}+a(n_{\mathrm{C}}^{\mathrm{th}})^2-b+1}. \tag{63}$$

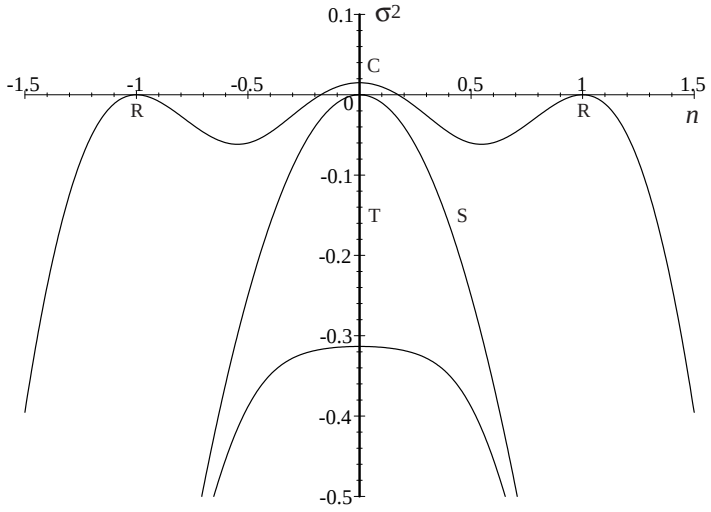

Fig. 6. The dispersion relation for $a = 1/2$, $b = 3/2$, $\rho = 0.97$, and $\gamma = 1$ (a slightly supercritical state of the tapelike regime).

Inserting expression (62) for $\mathbf{u}_C$ into (36) and computing the corresponding twist vector to first order using (31) yields

$$\kappa_1 = \varepsilon\ \gamma(n_C - \chi)(i A_C \exp i\gamma n_C s + \text{c.c.}), \tag{64.a}$$

$$\kappa_2 = \varepsilon\ \gamma(1 - n_C\chi)(A_C \exp i\gamma n_C s + \text{c.c.}), \tag{64.b}$$

$$\kappa_3 = \gamma, \tag{64.c}$$

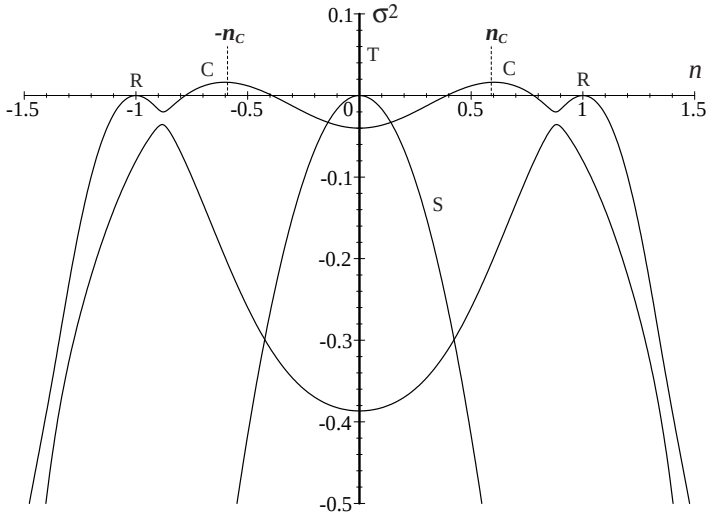

Fig. 7. The dispersion relation for $a = \frac{1}{2}$, $b = \frac{5}{2}$, $\rho = 2.08$, and $\gamma = 1$ (a slightly supercritical state of the thick regime).

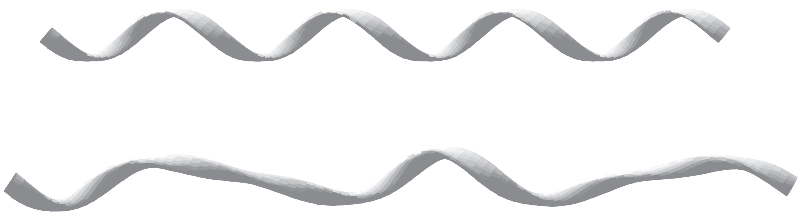

Fig. 8. Strips in coiled state for tapelike regime values ($a = 1/10$, $b = 2/11$, upper picture) and thick regime values ($a = 7/20$, $b = 14/27$, lower picture) of the material parameters. The shape of the strip is a helix in the tapelike case, but not in the thick case.

where A_C is an arbitrary complex amplitude. We choose to write the real neutral C mode (64) in both regimes as a sum of two complex conjugate modes, even for zero critical frequency n_C, in order to adopt a uniform notation. If $n_C = 0$, the imaginary part of the complex amplitude A_C is irrelevant, because the solution depends on A_C only through the combination $A_C + A_C^*$. Therefore, in the tapelike regime, we conventionally set $\mathrm{im} A_C$ to zero.

In the tapelike regime, taking into account the fact that $n_C = \chi = 0$, the twist vector reduces to

$$\kappa = \varepsilon\ \gamma \mathrm{Re} A_C\ \mathbf{d}_2 + \gamma\ \mathbf{d}_3. \tag{65}$$

Moreover, it is easily checked that $\mathbf{F} = (b - a)\gamma\kappa$. From (24), we see that the neutral C mode in the tapelike regime is just a binormal helix with torsion γ and curvature $\varepsilon\ \gamma A_C$ (see Figure 8). This tendency of the strip to assume the shape of a binormal helix has been termed *tapelike behavior* by van der Heijden et al. [40].

In the symmetric case $a = 1$, $\chi = \mathrm{sgn}(2 - b) = \pm 1$, and (64) reduces to

$$\kappa_1 = \varepsilon\ \gamma(n_C \mp 1)(i A_C \exp i\gamma n_C s + \text{c.c.}), \tag{66.a}$$

$$\kappa_2 = \varepsilon\ \gamma(1 \mp n_C)(A_C \exp i\gamma n_C s + \text{c.c.}), \tag{66.b}$$

$$\kappa_3 = \gamma. \tag{66.c}$$

The Frenet curvature and torsion are constant; hence, the C mode in the case $a = 1$ once again describes a helix, but this time with a constant twist density which differs from pure torsion.

In the thick regime, for $a \neq 1$, the expressions (64) describe buckling states for which the strip does not assume a helical shape (see Figure 8).

To summarize, as the control parameter ρ decreases from the region of stability and meets its critical value ρ_C, a neutral mode of type (64) (the neutral C mode) appears and, as ρ crosses the critical value, the appearance of unstable exponentially growing modes invalidates the linear description of the strip near the straight state. It is then necessary to proceed to a nonlinear analysis of these buckling modes.

4. Nonlinear Analysis

Our goal in this section is to study the behavior of the linearly unstable C modes and their interactions with other excitable or neutral modes in the nonlinear regime. An important effect of the nonlinearities is to curb the exponential growth of the C modes, allowing the system to eventually reach a new stable state or to oscillate between different states. The nonlinear analysis consists of studying the system close to the bifurcation in a regime where the perturbation parameter ε provides an effective measure of the distance to the critical point. It is then possible to study the dynamics in a systematic manner by expanding the Kirchhoff equations order by order in ε to obtain a hierarchy of linear equations. Furthermore, the amplitudes of the neutral modes are allowed to vary on long space and time length scales. To third order in this hierarchy, one can extract, as a solvability condition, a system of *amplitude equations*—namely, a system of equations governing the dynamics of the amplitude of the C mode (plus other relevant normal modes) that captures the essential nonlinear effects. These methods, first introduced in hydrodynamics, have proved to be of great value in a host of physical problems [10], [12], [29], [30].

Once the amplitude equations are established, it becomes possible to consider a variety of problems of interest.

4.1. Principle Ingredients of the Nonlinear Analysis

4.1.1. Behavior Near Criticality. Near the bifurcation point, a continuum of unstable modes is allowed to grow, with spatial frequencies spread over a small interval centered around $n = n_C$ and slightly positive time exponents σ. It is easy to determine the spatial bandwidth δn, and the time exponent interval $\delta\sigma$, of the unstable modes as functions of the distance $\delta\rho = \rho - \rho_C$ separating the control parameter from its critical value ($\delta\rho < 0$ in the supercritical case). The order of magnitude of δn for small $-\delta\rho$ is given by the distance separating nearby real roots of (54), namely

$$(\delta n)^{\mathrm{TL}} \equiv 2\sqrt{\frac{\Sigma + \sqrt{\Delta}}{2a}}, \tag{67.a}$$

$$(\delta n)^{\mathrm{th}} \equiv \left| \sqrt{\frac{\Sigma + \sqrt{\Delta}}{2a}} - \sqrt{\frac{\Sigma - \sqrt{\Delta}}{2a}} \right|, \tag{67.b}$$

where $(\delta n)^{\mathrm{TL}}$ and $(\delta n)^{\mathrm{th}}$ denote the tapelike and thick regimes respectively, and where Δ and Σ are analytic functions of $\delta\rho$ defined in (55.a) and (55.b). In the tapelike regime $\Sigma + \sqrt{\Delta}$ is an analytic function of $\delta\rho$ which, to leading order, is linear in $\delta\rho$. In the thick regime Δ is also linear in $\delta\rho$ to leading order, and Σ tends to a nonzero value as $\delta\rho \to 0$. In both regimes we have

$$\delta n \sim \sqrt{-\delta\rho}. \tag{68}$$

A similar result for $\delta\sigma$ can be obtained from the dispersion relation (39) by studying the dependence of σ on $\delta\rho$ for $n = n_C$:

$$\delta\sigma \sim \sqrt{-\delta\rho}. \tag{69}$$

In order for δn and $\delta\sigma$ to be analytic in the perturbation parameter ε, it is necessary to consider states close enough to the critical point for the variation $\delta\rho$ in the control parameter to be of order ε^2.

4.1.2. Slowly Varying Amplitudes and Multiple Scales. The main idea behind the nonlinear analysis is to express the first-order solution of the Kirchhoff equations as a linear combination of a number of the normal modes considered in Section 3, with the constant complex amplitudes A_k being replaced by nonconstant amplitudes $A_k(s,t)$ which vary slowly with space and time. This enables one to take into account the slight dispersion of the spatial frequencies n and the time exponents σ around n_k and σ_k and $\delta\rho = 0$. Thus, we require

$$\frac{\partial}{\partial s}\left[A_k(s,t)\exp\gamma(\sigma_k t + i n_k s)\right] \sim i\gamma(n_k+\delta n)\ A_k(s,t)\exp\gamma(\sigma_k t + i n_k s), \tag{70}$$

by setting

$$\frac{\partial A_k}{\partial s} \sim \delta n\ A_k \sim \varepsilon\ A_k. \tag{71}$$

Similarly, we require that

$$\frac{\partial A_k}{\partial t} \sim \delta\sigma\ A_k \sim \varepsilon\ A_k. \tag{72}$$

This condition of slow dependence in space and time can be formalized by introducing new space and time variables describing the variations of the relevant functions on different scales,

$$s \sim s^{(0)} \sim \varepsilon^{-1}\, s^{(1)} \sim \varepsilon^{-2}\, s^{(2)} \sim \cdots, \tag{73.a}$$

$$t \sim t^{(0)} \sim \varepsilon^{-1}\, t^{(1)} \sim \varepsilon^{-2}\, t^{(2)} \sim \cdots, \tag{73.b}$$

and treating functions of s and t as if they depend on these new scales in an independent manner. The differential operators can then be expanded as sums of operators acting on the different scales:

$$\frac{\partial}{\partial s} \equiv \frac{\partial}{\partial s^{(0)}} + \varepsilon\ \frac{\partial}{\partial s^{(1)}} + \varepsilon^2\ \frac{\partial}{\partial s^{(2)}} + \cdots, \tag{74.a}$$

$$\frac{\partial}{\partial t} \equiv \frac{\partial}{\partial t^{(0)}} + \varepsilon\ \frac{\partial}{\partial t^{(1)}} + \varepsilon^2\ \frac{\partial}{\partial t^{(2)}} + \cdots. \tag{74.b}$$

Exponential factors are considered to vary only on the $s^{(0)}$ and $t^{(0)}$ scales, whereas the slowly varying amplitudes, $A_k(s,t)$, are taken to depend on the longer scales ($t^{(1)}$, $t^{(2)}$,..., $s^{(1)}$, $s^{(2)}$,...), and not on $s^{(0)}$ or $t^{(0)}$.

4.1.3. Relevant Normal Modes. Taking into account all the relevant modes, the first-order solution of the Kirchhoff equations takes the form,

$$\mathbf{X}^{(1)} = \sum_k A_k(s^{(1)}, s^{(2)}, \ldots, t^{(1)}, t^{(2)}, \ldots)\ \mathbf{u}_k \exp\gamma(\sigma_k t^{(0)} + i n_k s^{(0)}). \tag{75}$$

In theory, we should include in (75) the neutral C mode responsible for instability and all other modes which can interact with the C mode through nonlinear effects. In practice, however, we restrict the number of included modes by conjecturing that the fast oscillating modes, namely, the modes with $\sigma^2 < 0$ and $|\sigma| \gg |\varepsilon|$, can be omitted from the analysis. This assumption—which requires that all the observed phenomena are quasistatic—is presumed to hold in the course of an experiment where the control parameter ρ is gradually decreased from its critical value. In situations that are not quasi-static, it is more difficult to justify the absence of the oscillatory modes. Since the Kirchhoff equations describe a conservative system, we cannot expect these modes to be exponentially damped in time as in dissipative situations. However, a nonlinear analysis reveals in this case that these modes cannot become unstable by coupling with other modes and that they are only relevant in the dynamics if they are initially excited. Therefore, we consider physical situations, where these modes are not present in the dynamics.

As a consequence, we only retain neutral modes. There are four of them: the static T, S, R, and C modes. As we shall see, the S and T modes play a crucial role in the dynamics and cannot be omitted in the description, whereas it can be shown that the R mode decouples completely from the dynamics of the C and S modes. Hence, we drop the R mode dependence in the first-order solution as well.

4.1.4. The Fredholm Alternative. Expressions (74.a) and (74.b) can be used to obtain an expansion of the linear operator $\mathbf{L}$ appearing in equation (33):

$$\mathbf{L} \equiv \mathbf{L}^{(0)} + \varepsilon\, \mathbf{L}^{(1)} + \varepsilon^2\, \mathbf{L}^{(2)} + \cdots, \tag{76}$$

where the operators $\mathbf{L}^{(k)}$ with $k > 0$ involve derivatives with respect to the longer space and time scales. Expanding the Kirchhoff system order by order, we have

order ε^1:

$$\mathbf{L}^{(0)}\, \mathbf{X}^{(1)} = \mathbf{0}, \tag{77}$$

order ε^2:

$$\mathbf{L}^{(0)}\, \mathbf{X}^{(2)} = \mathbf{Q}_2^{(0)}[\mathbf{X}^{(1)}] - \mathbf{L}^{(1)}\, \mathbf{X}^{(1)}, \tag{78}$$

order ε^3:

$$\begin{aligned} \mathbf{L}^{(0)}\, \mathbf{X}^{(3)} = \mathbf{C}_3^{(0)}[\mathbf{X}^{(1)}] + \mathbf{Q}_3^{(0)}[\mathbf{X}^{(1)}, \mathbf{X}^{(2)}] \\ + \mathbf{Q}_3^{(1)}[\mathbf{X}^{(1)}] - \mathbf{L}^{(1)}\, \mathbf{X}^{(2)} - \mathbf{L}^{(2)}\, \mathbf{X}^{(1)}, \end{aligned} \tag{79}$$

...

where $\mathbf{C}_3^{(0)}$ is a cubic function of its arguments and contains derivatives with respect to the short (i.e., $s^{(0)}$ and $t^{(0)}$) scales, and the $\mathbf{Q}_i^{(k)}$'s are quadratic functions of their arguments and derivatives up to the $s^{(k)}$ and $t^{(k)}$ space and time scales.

The amplitude equations can be obtained by applying the *Fredholm alternative* to the third-order system: that is, by requiring that the third-order solution is spatially bounded. This ensures that the contribution of the third-order solution is one order of

magnitude smaller than the second-order contribution for all s and t. Therefore, the most important features of the dynamics are contained in the first- and second-order solutions, in conjunction with the amplitude equations extracted to third-order. To second order, the Fredholm alternative is identically satisfied. In view of (78) and of the condition for boundedness, which is discussed in the following paragraphs, it might appear that the equations resulting from the second-order system should contain quadratic terms in the amplitudes. However, due to symmetries of the system, these terms vanish identically. Therefore, the second-order system can always be solved, and the solution is bounded and can be expressed in terms of the first-order solution.

The condition for boundedness is imposed by requiring that the right-hand side of (79) is orthogonal to every vector in the null space of the operator adjoint to $\mathbf{L}^{(0)}$. We first define the inner product $\langle \mathbf{x} \mid \mathbf{y} \rangle$ between two vectors $\mathbf{x}$ and $\mathbf{y}$ functions of $s^{(0)}$ and $t^{(0)}$ as

$$\langle \mathbf{x} \mid \mathbf{y} \rangle \equiv \int_{-\infty}^{+\infty} ds^{(0)} \int_{-\infty}^{+\infty} dt^{(0)}\, \mathbf{x}^{+}\mathbf{y}, \tag{80}$$

where $\mathbf{x}^{+}$ denotes complex conjugate transpose of $\mathbf{x}$, i.e.,

$$\mathbf{x}^{+} \equiv (\mathbf{x}^{\top})^{*}. \tag{81}$$

An appropriate normalization of (80) will be introduced shortly. The adjoint operator $\left(\mathbf{L}^{(0)}\right)^{+}$ is defined the usual way, namely,

$$\left\langle \mathbf{x} \mid \mathbf{L}^{(0)}\, \mathbf{y} \right\rangle = \left\langle \left(\mathbf{L}^{(0)}\right)^{+}\, \mathbf{x} \mid \mathbf{y} \right\rangle \qquad \forall\, \mathbf{x}, \mathbf{y}. \tag{82}$$

The Fredholm alternative consists in imposing the condition

$$\langle \mathbf{Y} \mid \mathbf{Z} \rangle = 0 \quad \forall\, \mathbf{Y} :\, \left(\mathbf{L}^{(0)}\right)^{+}\, \mathbf{Y} = \mathbf{0}, \tag{83}$$

where the column vector $\mathbf{Z}$ stands for the right-hand side of (79). Since the normal modes in the null space of the adjoint operator $\left(\mathbf{L}^{(0)}\right)^{+}$ constitute a basis for that space, it is sufficient to impose the condition (83) for all vectors $\mathbf{Y}$ of the form

$$\mathbf{Y} = \mathbf{v} \exp \gamma(\sigma t^{(0)} + ins^{(0)}),$$

where σ is imaginary, n is real, and the pair σ, n satisfy the dispersion relation. Inserting this into (83) yields the simpler condition

$$\left\langle \mathbf{v} \exp \gamma(\sigma t^{(0)} + ins^{(0)}) \mid \mathbf{Z} \right\rangle = 0 \qquad \forall\, \sigma, \mathrm{n}, \mathbf{v} : \mathbf{v}^{+}\, \mathbf{M} = \mathbf{0}, \tag{84}$$

where the matrix $\mathbf{M}$ depends on σ and n as defined in (38). Furthermore, since we include only neutral modes in (75), the right-hand side $\mathbf{Z}$ of (79) is actually independent of $t^{(0)}$ and is consequently orthogonal to every normal mode with $\sigma \neq 0$. Hence, we can further simplify (84) by only considering the modes with $\sigma = 0$. This yields the final form of the Fredholm condition (with the proper normalization factor):

$$\lim_{L\to\infty} \frac{1}{2L} \int_{-L}^{+L} ds^{(0)}\, \mathbf{v}^{+}\, \mathbf{Z}\, \exp(-i\gamma n s^{(0)}) = 0 \qquad \forall\, \mathrm{n}, \mathbf{v}^{+} : \mathbf{v}^{+}\, \mathbf{M}|_{\sigma=0} = \mathbf{0}. \tag{85}$$

4.2. Derivation of the Amplitude Equations

4.2.1. The Complete First-Order Solution. Taking into account the explicit form of the three retained neutral modes near criticality, the first-order solution (75) reads

$$\mathbf{X}^{(1)} = A_{\mathrm{T}}\,\mathbf{u}_{\mathrm{T}} + A_{\mathrm{S}}\,\mathbf{u}_{\mathrm{S}} + (A_{\mathrm{C}}\,\mathbf{u}_{\mathrm{C}} \exp i\gamma n_{\mathrm{C}} s^{(0)} + \text{c.c.}). \tag{86}$$

Hence, the complete first-order solution is

$$F_1^{(1)} = -\chi\rho_{\mathrm{C}}\gamma^2(i A_{\mathrm{C}} \exp i\gamma n_{\mathrm{C}} s^{(0)} + \text{c.c.}), \tag{87.a}$$
$$F_2^{(1)} = \rho_{\mathrm{C}}\gamma^2(A_{\mathrm{C}} \exp i\gamma n_{\mathrm{C}} s^{(0)} + \text{c.c.}), \tag{87.b}$$
$$F_3^{(1)} = A_{\mathrm{T}}, \tag{87.c}$$
$$\alpha_1^{(1)} = (A_{\mathrm{C}} \exp i\gamma n_{\mathrm{C}} s^{(0)} + \text{c.c.}), \tag{87.d}$$
$$\alpha_2^{(1)} = \chi(i A_{\mathrm{C}} \exp i\gamma n_{\mathrm{C}} s^{(0)} + \text{c.c.}), \tag{87.e}$$
$$\alpha_3^{(1)} = A_{\mathrm{S}}. \tag{87.f}$$

The variation in control parameter is handled through the tension amplitude A_{T}. Since we consider only states of the rod for which the control parameter ρ departs from its critical value by a term of order ε^2, we set $A_{\mathrm{T}} = 0$, postponing a perturbative contribution of tension to second order. The first-order contributions to the components of the twist vector are given by (31) and read

$$\kappa_1^{(1)} = \gamma(n_{\mathrm{C}} - \chi)(i A_{\mathrm{C}} \exp i\gamma s^{(0)} + \text{c.c.}), \tag{88.a}$$
$$\kappa_2^{(1)} = \gamma(1 - n_{\mathrm{C}}\chi)(A_{\mathrm{C}} \exp i\gamma s^{(0)} + \text{c.c.}), \tag{88.b}$$
$$\kappa_3^{(1)} = 0. \tag{88.c}$$

That is, to first order, only the C mode affects the curvature, and the twist density is unchanged. Next, we compute the first-order contributions to the components of the tangent vector $\mathbf{d}_3$ in the fixed basis $(\mathbf{e}_{\mathrm{X}}, \mathbf{e}_{\mathrm{Y}}, \mathbf{e}_{\mathrm{Z}})$. Introducing

$$\hat{r} \equiv \mathbf{d}_3 \cdot (\mathbf{e}_{\mathrm{X}} + i\mathbf{e}_{\mathrm{Y}}), \tag{89.a}$$
$$z \equiv \mathbf{d}_3 \cdot \mathbf{e}_{\mathrm{Z}}, \tag{89.b}$$

and expanding

$$\hat{r} = \varepsilon\,\hat{r}^{(1)} + \varepsilon^2\,\hat{r}^{(2)} + \cdots, \tag{90.a}$$
$$z = 1 + \varepsilon\,z^{(1)} + \varepsilon^2\,z^{(2)} + \cdots, \tag{90.b}$$

we have

$$\hat{r}^{(1)} = -i\left[(1-\chi)\,A_{\mathrm{C}} \exp i\gamma n_{\mathrm{C}} s^{(0)} + (1+\chi)\,A_{\mathrm{C}}^{*} \exp -i\gamma n_{\mathrm{C}} s^{(0)}\right] \exp i\gamma s^{(0)}, \tag{91.a}$$
$$z^{(1)} = 0. \tag{91.b}$$

We now compute the first-order contribution to the centerline shape $\mathbf{R}(s, t)$. To do so, we have to evaluate integrals of type

$$\int ds\; A(s^{(1)}, s^{(2)}, \ldots) \exp i\gamma n s^{(0)}, \tag{92}$$

with $n \neq 0$. Therefore, To leading order, the integral (92) simplifies to

$$\int ds\ A(s^{(1)}, s^{(2)}, \ldots) \exp i\gamma n s^{(0)} = \frac{-i}{\gamma n} A(s^{(1)}, s^{(2)}, \ldots) \exp i\gamma n s^{(0)}. \tag{93}$$

Introducing for the centerline $\mathbf{R}$ a set of complex cylindrical coordinates defined as

$$\hat{R} \equiv \mathbf{R} \cdot (\mathbf{e}_X + i\,\mathbf{e}_Y) = \int ds\ \hat{r}, \tag{94.a}$$

$$Z \equiv \mathbf{R} \cdot \mathbf{e}_Z = \int ds\ z, \tag{94.b}$$

we obtain from (91) and (93)

$$\hat{R}^{(1)} = -\frac{1}{\gamma}\left[\frac{1-\chi}{1+n_C} A_C \exp(i\gamma n_C s^{(0)}) + \frac{1+\chi}{1-n_C} A_C^* \exp\,(-i\gamma n_C s^{(0)})\right] \exp i\gamma s^{(0)}, \tag{95.a}$$

$$Z^{(1)} = 0. \tag{95.b}$$

4.2.2. The Second-Order Solution. The general second-order solution is obtained by adding a particular solution to the general solution of the first-order (homogeneous) system. Only particular solutions are needed since, by redefining the first-order amplitudes, we can cancel the homogeneous contribution to the second-order solution. However, this does not hold for the tension because, having set $A_T = 0$, we must explicitly include a constant second-order contribution B_T to the tension, accounting for the possible variation of tension away from the boundary condition. We do not state explicitly the full second-order solution. Instead, we limit ourselves to giving expressions for quantities of interest describing leading-order perturbative effects, i.e., which do not have a first-order counterpart. Namely, the tension $F_3^{(2)}$, the twist density $\kappa_3^{(2)}$, the tangent vector component $z^{(2)}$, and the centerline coordinate $Z^{(2)}$ in the $\mathbf{e}_Z$ direction are given by

$$F_3^{(2)} = \gamma^2\left[-\Psi_T\ (A_C^2 \exp 2i\gamma n_C s^{(0)} + \text{c.c.})\right] + B_T, \tag{96.a}$$

$$\kappa_3^{(2)} = \gamma\left\{[2n_C\Psi_S - \frac{1}{2}(1-\chi^2)]\ (A_C^2 \exp 2i\gamma n_C s^{(0)} + \text{c.c.}) - (1 - 2n\chi + \chi^2)\ |A_C|^2\right\} + \frac{\partial A_S}{\partial s^{(1)}}, \tag{96.b}$$

$$z^{(2)} = -(1+\chi^2)\,|A_C|^2 - \frac{1-\chi^2}{2}\left(A_C^2 \exp 2i\gamma n_C s^{(0)} + \text{c.c.}\right), \tag{96.c}$$

$$Z^{(2),\mathrm{TL}} = -2\int ds A_C^2, \tag{96.d}$$

$$Z^{(2),\mathrm{th}} = \frac{1-\chi^2}{4\gamma n_C}\left(i\,A_C^2 \exp 2i\gamma n_C s^{(0)} + \text{c.c.}\right) - (1+\chi^2)\int ds\,|A_C|^2\,, \tag{96.e}$$

where (96.d) and (96.e) hold for the tapelike and thick regimes respectively, and Ψ_T and Ψ_S are given functions of a and b which vanish in the case $a = 1$ and over the whole

tapelike regime domain. In the thick regime, these coefficients take the form

$$\Psi_{\mathrm{T}}^{\mathrm{th}} \equiv \frac{1}{2}\rho_{\mathrm{C}}(1-\chi^2), \tag{97.a}$$

$$\Psi_{\mathrm{S}}^{\mathrm{th}} \equiv \frac{b(1-\chi^2)+(1-a)\left[1+\chi^2-\frac{\chi}{n_{\mathrm{C}}}(1+n_{\mathrm{C}}^2)\right]}{4bn_{\mathrm{C}}}. \tag{97.b}$$

The expressions (96.d) and (96.e) for $Z^{(2)}$ account for the contraction of the buckled ribbon in the $\mathbf{e}_Z$ direction due to inextensibility of the material.

4.2.3. Left Null Space of the Linearized Kirchhoff Operator. As mentioned in Section 4.1.4, we have to determine the left null space of the matrix $\mathbf{M}$ defined in (38) for $\sigma = 0$. Solving the equation

$$\mathbf{v}^+ \mathbf{M} = \mathbf{0}$$

for the row vector $\mathbf{v}^+$, we find six linearly independent solutions, two vectors $\mathbf{v}_{\mathrm{R}}^+$ corresponding to the R branch which we do not need in our analysis. For $n = 0$, we have

$$\mathbf{v}_{\mathrm{T}}^+ \equiv \begin{pmatrix} 0 & 0 & 1 & 0 & 0 & 0 \end{pmatrix}, \tag{98.a}$$

$$\mathbf{v}_{\mathrm{S}}^+ \equiv \begin{pmatrix} 0 & 0 & 0 & 0 & 0 & 1 \end{pmatrix}. \tag{98.b}$$

For $n = n_{\mathrm{C}}$, we have

$$\mathbf{v}_{\mathrm{C}}^+ \equiv \begin{pmatrix} \dfrac{i(\chi+2n_{\mathrm{C}}+n_{\mathrm{C}}^2\chi)}{(1-n_{\mathrm{C}}^2)^2} & \dfrac{1+2n_{\mathrm{C}}\chi+n_{\mathrm{C}}^2}{(1-n_{\mathrm{C}}^2)^2} & 0 & -\gamma^2 & i\gamma^2\chi & 0 \end{pmatrix}, \tag{99}$$

and finally, for $n = -n_{\mathrm{C}}$, we have the complex conjugate of (99).

4.2.4. The Amplitude Equations. We obtain the amplitude equations from (85), taking the three vectors (98)–(99) in turn as expressions for $\mathbf{v}^+$. The right-hand side of (79) being real, $\mathbf{v}_{\mathrm{C}}^+$ leads to the same equation as its complex conjugate. The equations corresponding to $\mathbf{v}_{\mathrm{T}}^+$, $\mathbf{v}_{\mathrm{S}}^+$, and $\mathbf{v}_{\mathrm{C}}^+$ are subsequently referred to as the *T, S, and C equations*, respectively.

A subtle point must be mentioned here: Applying the Fredholm condition to order 3, we find nontrivial C- and S-equations, although the T-equation is identically satisfied, leaving the amplitude B_{T} undetermined. In order to close the system, it is necessary to find a nontrivial T-equation by computing the Fredholm condition for $\mathbf{v}_{\mathrm{T}}^+$ to order 4. The computation is rather tedious, and not much could be gained by including it here, so that only the final results are given.

The C-, S-, and T-equations assume different although similar forms in the tapelike and thick regime. As stated before, in the tapelike regime, the imaginary part of A_{C} is meaningless. We may thus set it arbitrarily to zero, so that the equations read, in both regimes[3]

[3] The reader accustomed to amplitude equations might wonder about the absence of a linear term A_{C} in the r.h.s. of the first amplitude equation describing the main instability. This linear term is actually hidden in the definition of the amplitude B_{T} which describes, at the extremities of the rod, the variation of tension away from the critical value.

$$P\left(\frac{\partial^2}{(\partial t^{(1)})^2} - c_{\mathrm{C}}^2 \frac{\partial^2}{(\partial s^{(1)})^2}\right) A_{\mathrm{C}} = \gamma^2 A_{\mathrm{C}} \left[Q\left(\frac{1}{\gamma}\frac{\partial A_{\mathrm{S}}}{\partial s^{(1)}} - \frac{B_{\mathrm{T}}}{2\rho_{\mathrm{C}}\gamma^2}\right) - MN\ |A_{\mathrm{C}}|^2 \right], \tag{100.a}$$

$$(1+a)\left(\frac{\partial^2}{(\partial t^{(1)})^2} - c_{\mathrm{S}}^2 \frac{\partial^2}{(\partial s^{(1)})^2}\right) A_{\mathrm{S}} = -\gamma Q N \frac{\partial\, |A_{\mathrm{C}}|^2}{\partial s^{(1)}}, \tag{100.b}$$

$$\frac{\partial^2 B_{\mathrm{T}}}{(\partial s^{(1)})^2} = \left(-N(1+\chi^2)\frac{\partial^2}{(\partial t^{(1)})^2} - \rho_{\mathrm{C}}\gamma^2 \frac{\partial^2}{(\partial s^{(1)})^2}\right) |A_{\mathrm{C}}|^2, \tag{100.c}$$

where, as stated before, the T-equation (100.c) is obtained from the Fredholm condition to fourth order. These equations form a system of nonlinear Klein-Gordon equations coupling the C, S, and T modes, which are equivalent, provided time dependence is dropped, to the normal forms obtained by van der Heijden et al. [40]. The advantages of the amplitude-equation approach is that explicit relations have been obtained (in the previous section) between physical quantities and the variables involved in the reduced system. This allows for the investigation of practical problems (see Section 5). The fundamental role played by the S and T modes in the buckling process is now obvious: If we set $A_{\mathrm{S}} = 0$ or $B_{\mathrm{T}} = 0$ in (100), we see that A_{C} is constrained to have a fixed or traveling-wave-like modulus, restricting drastically the behavior of the solutions.

The constants c_{S}, M, N, and Q and the combination Pc_{C}^2 are all functions of the material parameters a and b, whereas the time-scale constant P is, in addition, an inhomogeneous function of the twist density γ. They are defined as follows. The twist velocity c_{S} is, as before, given by (42). The expressions for c_{C}, P, Q, N, and M are different in the two regimes. The tapelike regime values are

$$P^{\mathrm{TL}} \equiv 1 + \gamma^{-2}, \tag{101.a}$$

$$Q^{\mathrm{TL}} \equiv 2(b-a), \tag{101.b}$$

$$P^{\mathrm{TL}}(c_{\mathrm{C}}^{\mathrm{TL}})^2 \equiv 1 - \frac{(1+a-b)^2}{1-a}, \tag{101.c}$$

$$N^{\mathrm{TL}} \equiv 2, \tag{101.d}$$

$$M^{\mathrm{TL}} \equiv 2(b-a), \tag{101.e}$$

whereas the thick regime values are

$$P^{\mathrm{th}} \equiv 1 + a\chi^2 + \frac{(1+\chi^2)\,(1+n_{\mathrm{C}}^2) + 4n_{\mathrm{C}}\chi}{\gamma^2(1-n_{\mathrm{C}}^2)^2}, \tag{102.a}$$

$$Q^{\mathrm{th}} \equiv 2\rho_{\mathrm{C}}(1+\chi^2), \tag{102.b}$$

$$P^{\mathrm{th}}(c_{\mathrm{C}}^{\mathrm{th}})^2 \equiv \frac{4a\chi^2}{1+a\chi^2}, \tag{102.c}$$

$$N^{\mathrm{th}} \equiv 1, \tag{102.d}$$

$$M^{\mathrm{th}} \equiv \rho_{\mathrm{C}}(1+\chi^2)^2 - \frac{1}{8b}\left[b(1-\chi^2) + (1-a)\left(1+\chi^2 - \frac{(1+n_{\mathrm{C}}^2)\chi}{n_{\mathrm{C}}}\right)\right]$$

$$\left(\frac{(a-1)\chi}{n_C} + 1 - a\chi^2 + 7[b(1-\chi^2) + \chi^2 - a - (1-a)n_C\chi]\right)$$
$$+ \frac{1}{2}n_C^2(1+a\chi^4) + b(1+4n_C^2)\chi^2 + \left(\frac{3}{2} - 4n_C\chi\right)(b-a)$$
$$+ \left(\frac{3}{2}\chi - 4n_C\right)\chi^3(b-1) - (1+a)\left(\frac{1}{2} + \frac{5}{2}n_C^2\right)\chi^2. \qquad (102.e)$$

The buckling velocity c_C^2 is strictly positive everywhere except at the regime boundaries $b = b_\pm$, where it vanishes. The time-scale constant P and the coupling constants Q and M are strictly positive for all values of a, b, and γ.

Amplitude equations for $a = 1$**.** In the symmetric case, (100) reduces to

$$\left[\left(1 + \frac{4}{\gamma^2 b^2}\right)\frac{\partial^2}{(\partial t^{(1)})^2} - \frac{\partial^2}{(\partial s^{(1)})^2}\right] A_C$$
$$= \frac{b^2}{2}\, A_C\left(\gamma\frac{\partial A_S}{\partial s^{(1)}} - \frac{B_T}{2\rho_C} - b\gamma^2\,|A_C|^2\right), \qquad (103.a)$$
$$\left(\frac{\partial^2}{(\partial t^{(1)})^2} - \frac{b}{2}\frac{\partial^2}{(\partial s^{(1)})^2}\right) A_S = \frac{-\gamma b^2}{2}\frac{\partial\,|A_C|^2}{\partial s^{(1)}}, \qquad (103.b)$$
$$\frac{\partial^2 B_T}{(\partial s^{(1)})^2} = -2\left(\frac{\partial^2}{(\partial t^{(1)})^2} + \frac{b^2\gamma^2}{4}\frac{\partial^2}{(\partial s^{(1)})^2}\right)|A_C|^2. \qquad (103.c)$$

In the amplitude equations previously derived by Goriely and Tabor [16], we did not take into account the second-order variation of tension. The new amplitude equations derived here, which are the result of a fourth-order expansion, reveal the subtle nonlinear coupling of tension to the amplitude.

5. Buckling of Strips near Threshold

In this section, we proceed to an extensive analysis of the amplitude equations (100) in the static case (that is, we drop dependence in time). Since the notation is valid for both regimes (with the restriction that the imaginary part of A_C must be set to zero in the tapelike case), we discuss them in parallel. Indeed, unless explicitly mentioned, all subsequent results pertain to both regimes. In Section 5.1, we investigate briefly some particular infinite-length solutions, recovering and complementing Champneys, Thompson, and van der Heijden's results. In Section 5.2, we discuss in a general way an important class of finite-length, static solutions (i.e., clamped solutions). This allows us to introduce the necessary background for the treatment of three practical problems of interest, corresponding to different types of end loading, which we complete in Section 5.3. Since, in the previous section, we computed explicit forms for physical quantities in terms of the amplitudes, imposition of the boundary conditions becomes a transparent and easy task.

5.1. Infinite-Length Solutions of Interest

5.1.1. Spatially Uniform Strips. An important class of static, infinite solutions consists in the spatially uniform strips. We look for a solution to the system (100) of the form

$$A_{\mathrm{C}}(s^{(1)}, t^{(1)}) = |A_{\mathrm{C}}| \exp i\overline{k}s^{(1)}, \tag{104.a}$$

$$A_{\mathrm{S}}(s^{(1)}, t^{(1)}) = A_{\mathrm{S}}, \tag{104.b}$$

$$B_{\mathrm{T}}(s^{(1)}, t^{(1)}) = B_{\mathrm{T}}, \tag{104.c}$$

where $\overline{k}$ is a constant spatial frequency. In the tapelike regime, we must set k to zero because A_{C} is real. We find two distinct solutions, given by

$$(1) \quad |A_{\mathrm{C}}| = 0, \tag{105.a}$$

$$(2) \quad |A_{\mathrm{C}}| = \sqrt{-\frac{QB_{\mathrm{T}} + 2Pc_{\mathrm{C}}^2\overline{k}^2\rho_{\mathrm{C}}}{2MN\rho_{\mathrm{C}}\gamma^2}}. \tag{105.b}$$

The first one is, of course, the straight rod, which is unstable for $B_{\mathrm{T}} < 0$, and the second one is a supercritical, homogeneous buckling state which develops as the tension drops from its critical value.[4] As already mentioned and illustrated in Figure 8, in the thick regime, the buckling state is not helical for $a < 1$. In the tapelike regime, the bifurcating solution is an exact binormal helix, and (105.b) reduces to

$$|A_{\mathrm{C}}| = \frac{1}{2}\sqrt{-\frac{B_{\mathrm{T}}}{(b-a)\gamma^2}}, \tag{106}$$

where we have used (58), (101), and the fact that $\overline{k} = 0$ in the tapelike regime. Combining (106) with the second-order expressions (96.a) and (96.b), the binormal-helix relations (24) may be recovered, confirming this helical solution matches an exact feature of the Kirchhoff system.

5.1.2. Homoclinic Strips. Another important class of infinite solutions is the spatially homoclinic strips. Such buckling modes correspond to bounded, aperiodic solutions of the static amplitude equations. The time-independent form of the system (100) can be written in a more compact form. Indeed, we see that the static form of the S-equation (100.b) can be integrated once with respect to $s^{(1)}$, yielding

$$\frac{dA_{\mathrm{S}}}{ds^{(1)}} = \frac{\gamma QN\,|A_{\mathrm{C}}|^2}{b} + K_{\mathrm{S}}, \tag{107}$$

[4] At first sight, it might seem that the supercritical behavior of the homogeneous solution with tension taken as control parameter contradicts the results of Thompson and Champneys in [38], where it is demonstrated that helices are subcritical under dead loading. Actually, there is no contradiction, because our definition of the tension is different from that of Thompson and Champneys. They define the tension as the force exerted in the fixed $\mathbf{e}_{\mathrm{Z}}$ direction, whereas we define it as the tangential component of the force, which is not the same for helices.

where K_S is an integration constant. Similarly, the static form of the T-equation (100.c) may be integrated twice with respect to $s^{(1)}$,

$$B_T = -\rho_C \gamma^2 (1+\chi^2) N |A_C|^2 + K_T, \tag{108}$$

where we have introduced only one nonzero integration constant, K_T, in order to avoid unphysical terms linear in $s^{(1)}$. Substitution of (107) and (108) into the time-independent form of the C-equation (100.a) gives

$$\frac{2Pc_C^2}{\gamma^2 Q}\frac{d^2 A_C}{(ds^{(1)})^2} + \left[\left(\frac{2Q}{b} + 1 + \chi^2 - \frac{2M}{Q}\right) N |A_C|^2 + \frac{2K_S}{\gamma} - \frac{K_T}{\rho_C \gamma^2}\right] A_C = 0, \tag{109}$$

which is closed in A_C. Equations (107)–(109) may be further simplified by introducing the following definitions:

$$\nu \equiv \frac{2Pc_C^2}{Q}, \tag{110.a}$$

$$K_S \equiv \nu\gamma\overline{\gamma}, \tag{110.b}$$

$$K_T \equiv \nu\rho_C\gamma^2\overline{T}, \tag{110.c}$$

$$\mu \equiv \frac{3}{2}\left[1 + \frac{(1+\chi^2)b}{2Q} - \frac{Mb}{Q^2}\right], \tag{110.d}$$

$$A_C \equiv \sqrt{\frac{3b\nu}{4QN\mu}}\,\overline{A}. \tag{110.e}$$

Note that the definition (110.e) is valid only if $\mu > 0$. We have found that it is always the case except in a small, unphysical region of the (a, b) space corresponding to $b > 2$ and extremely low a. Therefore, from now on, we only consider the case $\mu > 0$. The final forms of the amplitude equations are, respectively,

$$\gamma^{-2}\frac{d^2\overline{A}}{(ds^{(1)})^2} - (\overline{T} - 2\overline{\gamma})\overline{A} + \left|\overline{A}\right|^2 \overline{A} = 0, \tag{111.a}$$

$$\frac{dA_S}{ds^{(1)}} = \gamma\nu\left(\overline{\gamma} + \frac{3\left|\overline{A}\right|^2}{4\mu}\right), \tag{111.b}$$

$$B_T = \rho_C\gamma^2\nu\left[\overline{T} - \frac{3(1+\chi^2)b\left|\overline{A}\right|^2}{4Q\mu}\right]. \tag{111.c}$$

The new C-equation (111.a) is closed in the variable $\overline{A}$, while the new S-equation (111.b) and T-equation (111.c) show that the twist and tension amplitudes A_S and B_T are driven passively by the buckling amplitude $\overline{A}$.

The equation for $\overline{A}$ (111.a) admits a family of spatially localized solutions of the form

$$\overline{A} = \sqrt{2(\overline{T} - 2\overline{\gamma})}\,\exp i\varphi\,\operatorname{sech}\gamma\sqrt{\overline{T} - 2\overline{\gamma}}s^{(1)}, \tag{112}$$

where φ is a constant phase that is arbitrary in the thick regime and takes the value 0 or π in the tapelike regime. Note that these solutions are defined only if $\overline{T} - 2\overline{\gamma} > 0$. From

(111) in conjunction with the first- and second-order solutions computed in Section 4, it can be shown that this condition implies $F_3/\kappa_3^2 > \rho_C$ at infinity. Therefore, all solutions of the form (112) are subcritical. This is in accordance with results of van der Heijden et al. [7], [39], [40], which demonstrate numerically (and confirm analytically in [40] through a normal-form analysis) the existence of subcritical, spatially homoclinic solutions. Additionally, in the case of a noncircular cross section, they show numerical evidence of multimodal homoclinic orbits. Such solutions lie beyond the scope of dominant-order amplitude equations. Their investigation might be considered by pursuing the nonlinear analysis of Section 4 to obtain higher-order coupling terms in the system.

5.2. Clamped, Finite-Length Solutions

We now focus on the more practical case of finite-length strips subject to given boundary conditions. Two classes of end-constraints may be considered:

Supported strip: the positions in space of both strip extremities are imposed (i.e., either fixed in place or moved during the course of an experiment), but the directions in space of the tangents to the strip at the ends are free, unconstrained parameters.

Clamped strip: the positions in space of both strip ends are imposed and, additionally, the tangents to the strip are constrained to face each other, that is, to, be lined up.

We consider only the clamped case, which is especially easy to implement at the level of the amplitude equations. Furthermore, we make the assumption that the strip length is much greater than the characteristic twist length γ^{-1}. One elegant way to formalize this is to define the so-far unspecified order parameter ε as

$$\varepsilon \equiv (\gamma L)^{-1}, \tag{113}$$

where L is the length of the strip. We refer to this limit as to the *large-twist-angle limit*, since the quantity in the right-hand side of (113) is the inverse of the angle between the unperturbed local bases at strip extremities, that is, 2π times the number of twist turns. We specify the arclength parameter origin so that

$$s \equiv s^{(0)} \equiv \varepsilon^{-1} s^{(1)} = \pm \frac{L}{2} \equiv \pm (2\gamma\varepsilon)^{-1} \tag{114}$$

at strip ends. We need to impose that the tangent vectors at the boundaries, $\mathbf{d}_3(\pm L/2)$, are parallel to each other and, additionally, that they are parallel to the vector $\mathbf{R}(L/2) - \mathbf{R}(-L/2)$ joining the strip extremities. Using expressions (91) and (95) giving the first nontrivial contributions to $\mathbf{d}_3$ and $\mathbf{R}$, we find that the condition for a clamped strip is equivalent to

$$A_C\left(\pm(2\gamma)^{-1}\right) = 0 \Longleftrightarrow \overline{A}\left(\pm(2\gamma)^{-1}\right) = 0, \tag{115}$$

which, in addition, implies that the tangent vectors lie in the $\mathbf{e}_Z$ direction. It can be shown that solutions to the static C-equation (111.a) vanishing at given points have a constant phase. An important consequence of this is that, under the condition of clamped ends, there is no distinction to be made, at least to leading order, between the tapelike and thick regime problems. Indeed, the boundary conditions freeze the value of the

phase of the Hamiltonian Hopf bifurcation to a constant value, and this phase is the only extra degree of freedom of the thick regime with respect to the tapelike regime. Furthermore, the constant value of the phase cannot be determined from amplitude equations or boundary conditions, so that there is no distinction to be made between regimes in subsequent results. Nevertheless, the value of the phase is needed in order to reconstruct the geometry of the strip in the thick regime. Surprisingly, the phase cannot be obtained from the leading order amplitude equations (111). The proper thing to do would be to introduce second-order contributions to the normal mode amplitudes and apply higher-order Fredholm conditions. This would yield small corrections to the amplitude equations, eventually allowing the determination of the phase.

We now need to find nontrivial solutions of the C-equation (111.a) vanishing at at least two distinct and opposite values of the arclength parameter. They are found to form a one-parameter family of periodic solutions which may be written in terms of Jacobi's elliptic function cn,

$$|\overline{A}| = k\sqrt{\frac{2(\overline{T}-2\overline{\gamma})}{2k^2-1}}\left|\mathrm{cn}\left(\sqrt{\frac{\overline{T}-2\overline{\gamma}}{2k^2-1}}\gamma s^{(1)} \mid k\right)\right|, \tag{116}$$

where the elliptic modulus k is a constant ranging in the interval $]0,1[$. We assume that the stable bifurcating solution is the fundamental one, that is, the solution whose amplitude vanishes only at the strip ends and does not create additional nodes along the strip. Taking into account (114) and introducing the *complete elliptic integral of the first kind* $\mathrm{K}(k)$, which gives the zeroes of the function cn as $(1+2l)\mathrm{K}(k)$, $l \in \mathbb{Z}$, we may relate the modulus k to the constants $\overline{T}$ and $\overline{\gamma}$:

$$\overline{T} - 2\overline{\gamma} = 4\mathrm{K}(k)^2(2k^2-1). \tag{117}$$

Substituting (117) into (116) yields

$$|\overline{A}| = |\overline{A}|_{\max}\left|\mathrm{cn}\left(2\mathrm{K}(k)\gamma s^{(1)} \mid k\right)\right|, \tag{118}$$

with

$$|\overline{A}|_{\max} \equiv 2\sqrt{2}k\mathrm{K}(k). \tag{119}$$

From the last equation, we see that the elliptic modulus k is a growing function of the maximum value of the buckling amplitude, $|\overline{A}|_{\max}$, taking the limits 0 for $|\overline{A}|_{\max} \to 0$ and 1 for $|\overline{A}|_{\max} \to \infty$. This means that the buckling mode becomes more and more localized as it develops. Indeed, the function cn deforms continuously from a cosine function for $k = 0$ into a fully localized sech function as k approaches unity, so that the spatially homoclinic solution of Section 5.1.2 is recovered. This result sheds new light onto a problem addressed by Thompson and Champneys in [38], in the case of rods with circular cross sections. They raise the question: which, of the helical solution of Love [26] and the localized solution of Coyne [9], is the preferred buckling mode under given boundary conditions? Their approach consists in comparing energetically the localized solution with the infinite, unmodulated helix, which is argued to be a valid approximation away from the rod boundaries. Their conclusions, confirmed by experiments, support

the idea of an initial helical mode which is quickly replaced by a localized mode along the bifurcation path. Here, we take into account the finiteness of the rod in a rigorous manner and find, in the clamped case, a smooth and quick deformation from an initial sinusoidally modulated helix into a localized configuration (see Figure 13). Hence, we recover previous results, but with the additional information that the process of mode-switching is continuous rather than involving a secondary bifurcation.

We now compute several quantities of interest for the purpose of solving the practical problems described below. Taking into account the boundary conditions (115), we obtain, from (96), (101.d), and (102.d), the twist density κ_3^{ends} and the tension F_3^{ends} at the strip extremities, as well as the distance $Z^{\text{ends}} = Z(L/2) - Z(-L/2)$ between end points:

$$\kappa_3^{\text{ends}} = \gamma + \varepsilon^2 \left(\frac{dA_{\text{S}}}{ds^{(1)}} \right)^{\text{ends}} + \text{o}(\varepsilon^2), \tag{120.a}$$

$$F_3^{\text{ends}} = \rho_{\text{C}} \gamma^2 + \varepsilon^2 B_{\text{T}}^{\text{ends}} + \text{o}(\varepsilon^2), \tag{120.b}$$

$$Z^{\text{ends}} = L - \varepsilon N (1 + \chi^2) \int_{-(2\gamma)^{-1}}^{(2\gamma)^{-1}} ds^{(1)} \, |A_{\text{C}}|^2 + \text{o}(\varepsilon). \tag{120.c}$$

In addition, the total twist angle ϑ^{ends} between strip ends may be shown, using (113), to admit the expansion,

$$\vartheta^{\text{ends}} = \varepsilon^{-1} + \varepsilon \left[A_{\text{S}} \left(\frac{1}{2\gamma} \right) - A_{\text{S}} \left(-\frac{1}{2\gamma} \right) \right] + \text{o}(\varepsilon). \tag{121}$$

We now introduce the definition,

$$\overline{Z} = -\gamma \int_{-(2\gamma)^{-1}}^{(2\gamma)^{-1}} ds^{(1)} \left| \overline{A} \right|^2, \tag{122}$$

which, from (118) and (119), may be evaluated in terms of k, taking into account elementary properties of elliptic functions,

$$\overline{Z} = 8\text{K}(k)^2 \left(1 - k^2 - \frac{\text{E}(k)}{\text{K}(k)} \right), \tag{123}$$

where $\text{E}(k)$ is the *complete elliptic integral of the second kind*. Using (122) together with the definition (110.e), the static amplitude equations (111), and the boundary conditions (115), we may express (120)–(121) in terms of the constants $\overline{T}$, $\overline{\gamma}$, and $\overline{Z}$:

$$\kappa_3^{\text{ends}} = \gamma (1 + \varepsilon^2 \nu \overline{\gamma}) + \text{o}(\varepsilon^2), \tag{124.a}$$

$$F_3^{\text{ends}} = \rho_{\text{C}} \gamma^2 (1 + \varepsilon^2 \nu \overline{T}) + \text{o}(\varepsilon^2), \tag{124.b}$$

$$Z^{\text{ends}} = L \left[1 + \varepsilon^2 \frac{3(1 + \chi^2) b \nu \overline{Z}}{4 Q \mu} + \text{o}(\varepsilon^2) \right], \tag{124.c}$$

$$\vartheta^{\text{ends}} = \varepsilon^{-1} \left[1 + \varepsilon^2 \nu \left(\overline{\gamma} - \frac{3\overline{Z}}{4\mu} \right) + \text{o}(\varepsilon^2) \right]. \tag{124.d}$$

The quantities $\overline{\gamma}$, $\overline{T}$, and $\overline{Z}$ have now a clear physical meaning: They are proportional to dominant-order nontrivial contributions to, respectively, the end torque $M_3^{\text{ends}} = b\kappa_3^{\text{ends}}$, the end tension, and the distance between strip extremities. They have been defined in such a way that the formulation of the results of the Section 5.3, where we consider practical problems, is as simple and universal as possible.

5.3. Three Practical Problems of Interest

In order to describe a real experiment, we must specify, in addition to the strip-clamping condition (115), the type of *loading* that we impose at strip ends, that is, whether the values of the parameters $\overline{T}$, $\overline{\gamma}$, $\overline{Z}$, and ϑ^{ends} are determined by stress or geometrical constraints. Indeed, the type of loading determines crucially the bifurcation scenario beyond the criticality [38]. This is confirmed by our finite-length results. We investigate three cases corresponding to different types of loading and find that the buckled strip presents very dissimilar behaviors.

5.3.1. Dead Loading. The first problem that we consider is the case of dead loading at the strip extremities. That is, we impose the values of the torque $\overline{\gamma}$ and the tension $\overline{T}$ at the ends, one of which is held fixed and the other one is controlled in the course of the experiment, and we allow the distance $\overline{Z}$ and the twist angle ϑ^{ends} to vary passively in response to changes in the control parameters.

It is straightforward to obtain a bifurcation diagram for the system under this set of boundary conditions: We simply plot the maximum of the buckling amplitude, $\left|\overline{A}\right|_{\max}$, against $2\overline{\gamma} - \overline{T}$, which we take as a control parameter. Parametric expressions for both quantities as functions of k are provided by (117) and (119). Figure 9 shows the resulting diagram. One of its most remarkable features is its universal character: Indeed, it only depends on the assumption that the strip is clamped and in the large-twist-angle limit. Another noticeable point is the fact that the bifurcation is subcritical. As a consequence, there exists no stable bifurcating branch connecting continuously to the reference (straight) state. The lack of a stable static solution beyond the bifurcation point implies that the system must perform a dynamical jump right after the bifurcation in order to reach a distant equilibrium state.

5.3.2. Rigid Loading. The second problem considered is the case of rigid loading: Here, the twist angle ϑ^{ends} is held fixed to its initial value, while the distance $\overline{Z}$ between strip ends is controlled during the experiment. The dynamical quantities $\overline{\gamma}$ and $\overline{T}$ are passive parameters.

A bifurcation diagram is obtained by plotting the maximum buckling amplitude $\left|\overline{A}\right|_{\max}$ against the end shortening, $-\overline{Z}$, for which a parametric expression is provided by (123). The diagram is shown in Figure 10, which is, once again, universal. Here, the straight strip adopts quasistatically a stable buckled state which develops as the strip ends are brought closer to each other. Figure 13 represents the bifurcating solution for several values of the distance between strip ends. The crucial role played by the boundary conditions is now obvious: This behavior is completely different from the dynamical jump predicted in the case of dead loading.

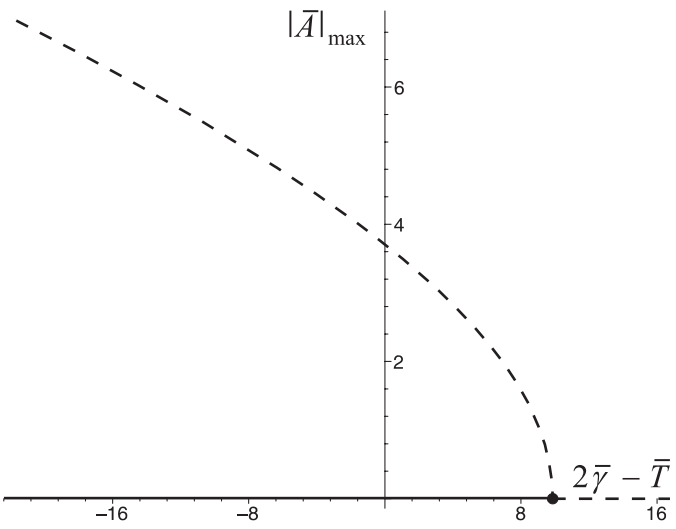

Fig. 9. Bifurcation diagram for a clamped strip with dead loading: maximum of the buckling amplitude as a function of end torque and tension.

5.3.3. Mixed Loading. The last case that we investigate is also the richest one. Here, we consider a mixed set of boundary conditions constituted of one geometrical constraint and one stress constraint. Namely, we keep the twist angle ϑ^{ends} fixed to its reference value, ε^{-1}, and control the tension $\overline{T}$. The parameters $\overline{\gamma}$ and $\overline{Z}$ are passive.

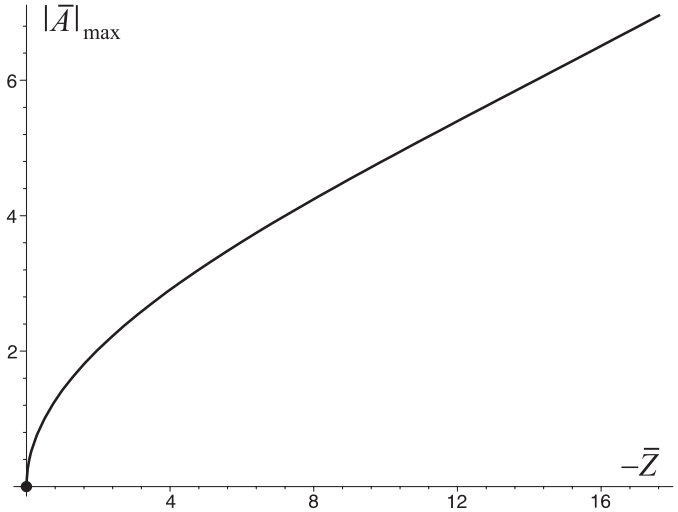

Fig. 10. Bifurcation diagram for a clamped strip with rigid loading: maximum of the buckling amplitude as a function of end shortening for fixed twist angle.

Keeping the twist angle fixed to the value ε^{-1} implies, from (124.d), that

$$\overline{\gamma} = \frac{3\overline{Z}}{4\mu}. \tag{125}$$

Substituting this into (117) yields an expression for the control parameter $\overline{T}$ as a function of k:

$$\overline{T} = -4\mathrm{K}(k)^2 \left[1 - 2k^2 + \frac{3}{\mu} \left(k^2 - 1 + \frac{\mathrm{E}(k)}{\mathrm{K}(k)} \right) \right], \tag{126}$$

which, together with (119), is used to build a bifurcation diagram. We point out that, unlike in the previous cases, the bifurcation diagram is not universal, but depends on the material parameters a and b through the constant μ. Consequently, we have to discuss the set of possible behaviors depending on the value of μ. To this end, we first determine the subcritical or supercritical character of the bifurcation as a function of μ. The bifurcation is subcritical if (126) defines a growing function of k at the origin $k = 0$. On the other hand, the bifurcation is supercritical if (126) defines a decreasing function of k at the origin. Computing the Taylor series of (126) about $k = 0$ to order 2 reveals that the bifurcation is supercritical if

$$0 < \mu < 1, \tag{127}$$

and, subcritical if

$$\mu \geq 1. \tag{128}$$

Hence, for $\mu \geq 1$, there is no stable static solution beyond the bifurcation point, so that the system must perform a dynamical jump, such as in the case of dead loading. On the other hand, for $\mu < 1$, there exists a stable, supercritical buckled state emerging from the straight solution at the bifurcation point. The boundary $\mu = 1$ in (a, b) space is represented in Figure 1 as the common edge of the white and light gray regions. A simple analytical expression for this boundary is obtained as a small-a expansion,

$$b = \frac{66}{49}a + \frac{60288}{420175}a^2 + \mathrm{O}(a^3), \tag{129}$$

which remains a good approximation throughout the physical parameter range. The supercritical case $\mu < 1$ presents an additional striking feature, which is illustrated in Figure 11, representing the bifurcation diagram in the particular case $\mu = 2/3$. We see here that the bifurcating branch possesses a second critical point at a finite value of the control parameter $\overline{T}$, beyond which it folds back subcritically. We give an interpretation of this fact in the next paragraph. For now, we establish a proof of the existence and uniqueness of this folding point in the interval $\mu \in]0, 1[$. The existence of the folding point is established by the observation that (126) defines a function of k which is decreasing at $k = 0$, but which goes to positive infinity in the limit $k \to 1$. In order to prove the uniqueness of the folding point, we first derive a relation between μ and the value of k at the folding point. This is achieved by differentiating the right-hand side of (126) with respect to k, equating the result to zero, and solving for μ. This relation, together with (119), provides parametric expressions of the buckling amplitude at the folding (limit)

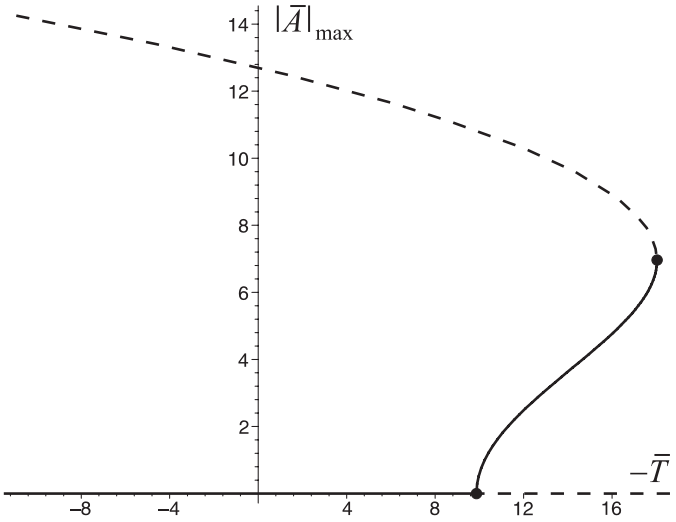

Fig. 11. Bifurcation diagram for a clamped strip with mixed loading ($\mu = 2/3$): maximum of the buckling amplitude as a function of tension for fixed twist angle.

point, $|\overline{A}|^{\mathrm{LP}}_{\max}$, as a function of μ. Graphical inspection of this relation (see Figure 12) reveals the uniqueness of the value of the amplitude at the folding point for given μ.

We now discuss the implications of the existence of a folding point in the bifurcation diagram. As mentioned before, for $\mu < 1$, a stable buckling state emerges from the straight state after it has lost its stability, and develops as the tension $\overline{T}$ is lowered. At

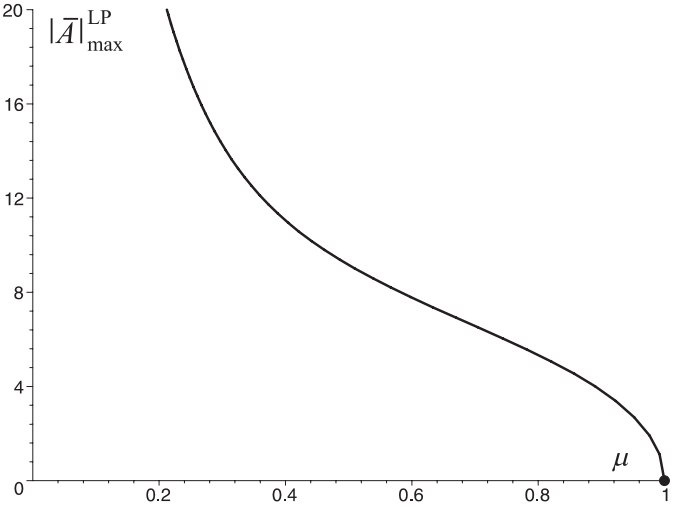

Fig. 12. Maximum of the buckling amplitude at the mixed-loading limit point as a function of μ.

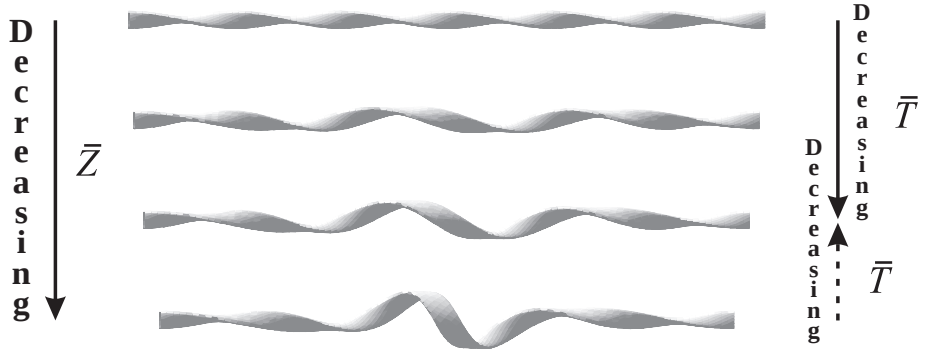

Fig. 13. Coiling of a clamped strip with fixed twist angle as tension or end shortening is varied. The parameter values are $a = 1/10, b = 2/11 \Rightarrow \mu = 2/3$, and belong to the tapelike regime. The diagrams are obtained using the explicit expressions for the strip shape derived in Section 5. The two arrows on the right-hand side of the diagram corresponds to the two different buckling paths of Figure 11. The dash line corresponds to the upper branch of the bifurcation diagram when a decrease of the amplitude is obtained by decreasing the tension, and the solid line follows the lower part of the bifurcation curve and corresponds to the buckling to a modulated helical strips form a straight rod.

the folding point, provided that the buckling state remains stable up to there, a minimal value of the tension is reached below which there exists no stable static state, and the system is forced to perform a dynamical jump. Consequently, the folding point marks a secondary bifurcation, a so-called *limit-point bifurcation*. This implies that the upper part of the bifurcating branch (above the limit point) is unstable. Figure 13 shows the buckled strip for $\mu = 2/3$ and several values of the tension. The third picture downwards in the figure corresponds to the limit-point value of the tension.

We assumed that the buckling mode remained stable up to the limit point. Now we give arguments in favor of this. To this end, we need to linearize the full, dynamical amplitude equations (100) about the equilibrium solution, and look for normal modes of the form

$$\mathbf{x}(s^{(1)}, t^{(1)}) = \overline{\mathbf{x}}(s^{(1)}) \exp \overline{\sigma} t^{(1)}, \tag{130}$$

where $\mathbf{x}$ is a compact notation for the set of dynamical variables involved in the linearized amplitude equations. As usual, the stability of the equilibrium solution is determined by the analysis of the allowed eigenvalues $\overline{\sigma}$. The existence of a solution to the linearized system satisfying the boundary conditions and corresponding to an eigenvalue with positive real part is a necessary and sufficient condition for the equilibrium solution to be unstable. Hence, the onset of instability is determined by the investigation of eigenvalues with zero real part. Two cases are considered:

Quasistatic bifurcation ($\mathrm{Re}\overline{\sigma} = 0, \mathrm{Im}\overline{\sigma} = 0$***).*** This occurs at points of the bifurcation diagram where either two branches of static solutions meet, or one branch folds back. The only points matching this criterion are the two bifurcations identified above (buckling and limit points). There exists no other quasistatic bifurcation.

Temporal Hamiltonian Hopf bifurcation (degenerate $\overline{\sigma}$ with $\mathrm{Re}\overline{\sigma} = 0, \mathrm{Im}\overline{\sigma} \neq 0$***).*** This corresponds to the onset of sustained temporal oscillations. We argue here that this type of bifurcation is unlikely to happen. Indeed, such a bifurcation involves the coalescence of two purely imaginary eigenvalues, one of them acquiring a positive real part as the control parameter bypasses a critical value. The main idea behind our argument is to consider the effect of a very small dissipation in the system. Independently of the way the dissipation term is introduced in the amplitude equations, if it is sufficiently small, we expect the eigenvalues to be nearly unchanged with respect to the conservative case. In particular, we expect the imaginary part of the eigenvalue which loses stability to remain nonzero. This, in turn, implies the existence of periodic solutions in a neighborhood of the bifurcation, even in the damped case. This would mean that a damped strip with static boundary conditions could sustain oscillations without energy input. Hence, we conjecture that the weak-amplitude buckling branch remains stable up to the limit point.

6. Conclusions

In this paper, we derived amplitude equations governing the dynamics of strips near the onset of twist instability. In Section 3, we performed a dynamical linear analysis of the Kirchhoff equations for strips around the straight solution. We identified several modes of wave propagation, namely, flexural and torsional waves (called respectively *R* and *S* modes). The R mode is found to be responsible for the pop-out of rods subject to longitudinal compression. Furthermore, below a critical tension-to-squared-twist, the straight strip becomes dynamically unstable. This result generalizes Love's criterion for the stability of twisted rods. Two distinct regimes of bifurcation are identified. In the case of very asymmetric cross sections with a high torsional stiffness, we found a regime of pitchfork bifurcation, inducing what van der Heijden et al. termed *tapelike behavior*. This corresponds to a bifurcating solution (*C mode*) assuming the shape of a binormal helix, as defined in the beginning of Section 3. In the other cases, the bifurcation is a Hamiltonian Hopf bifurcation, and the postinstability solution is not helical (except in the case of circular cross sections, as discovered by Love).

In Section 4, we performed a nonlinear analysis of the dynamical Kirchhoff equations for twisted straight strips in a state close to bifurcation. The resulting amplitude equations are a set of three nonlinear Klein-Gordon equations coupling the twist density and the longitudinal tension to the writhing C mode responsible for the buckling of twisted strips. The flexural, twist-independent, R mode decouples completely from the C and S modes. These equations provide the starting point for the analysis of a large variety of problems, such as the investigation of traveling waves or the determination of the equilibrium shape assumed by the strip under given boundary constraints. As an important example, we examined in detail the buckling of a finite-length strip clamped at the ends, in the large-twist-angle limit, for three different types of loading at the strip extremities. We found that, in the case of dead loading, the strip performs a dynamical jump at the bifurcation point, whereas under rigid loading, a stable buckling mode sets up beyond the criticality. The new equilibrium solution is found to deform continuously from a sinusoidally modulated helix into a localized solution along the bifurcation path. The third type of loading considered involves a geometrical constraint (fixed twist angle)

and a dynamical constraint (controlled tension). In this particular setting, the bifurcation path may be either subcritical or supercritical depending on material parameters and, in the latter case, presents a secondary bifurcation (a limit point) beyond which the system is forced to perform a dynamical jump. Arguments are given in favor of the stability of the buckling solution up to the limit point.

Future plans involve the analysis of time-dependent features of the amplitude equations for the twisted strip derived here. We hope that it will reveal new dynamical behavior such as breathers and traveling wave solutions. The bulk of the analysis performed here can then be directly used in this more general setting.

Acknowledgments

A. G. would like to thank A. Champneys, G. van der Heijden, and J. M. Thompson for interesting discussions and for providing him with unpublished materials. M. N. acknowledges support from the Fonds National de la Recherche Scientifique (FNRS) where he is an Aspirant. A. G. is a Sloan fellow whose work is supported by the NSF grant DMS-9972063 (A. G.) and NATO-CRG 97/037. M. T. also acknowledges support of the Flinn Foundation, NSF grant DMS-9704421 and EPSRC (U.K.) grant GR/M7/1886/01.

References

[1] S. S. Antman and C. S. Kenney. Large buckled states of nonlinearly elastic rods under torsion, thrust and gravity. *Arch. Rat. Mech. Anal.*, **84**, 289–338, 1981.

[2] S. S. Antman. *Nonlinear problems of elasticity*. Springer-Verlag, New York, 1995.

[3] M. D. Barkley and B. H. Zimm. Theory of twisting and bending of chain macromolecules. Analysis of the fluorescence depolarization of DNA. *J. Chem. Phys.*, **70**, 2991–3006, 1979.

[4] W. R. Bauer, R. A. Lund, and J. H. White. Twist and writhe of a DNA loop containing intrinsic bends. *Proc. Natl. Acad. Sci.*, **90**, 833–837, 1993.

[5] C. J. Benham. Theoretical analysis of conformational equilibria in superhelical DNA. *Ann. Rev. Biophys. Chem.*, **14**, 23–45, 1985.

[6] A. R. Champneys and J. M. T. Thompson. A multiplicity of localized buckling modes for twisted rod equations. *Proc. Roy. Soc. Lond. A*, **452**, 2467–2491, 1996.

[7] A. R. Champneys, G. H. M. van der Heiden, and J. M. T. Thompson. Spatially complex localisation after one-twist-per-wave equilibria in twisted rod circular rods with initial curvature. *Phil. Trans. Roy. Soc. A*, **355**, 2151–2174, 1997.

[8] B. D. Coleman, E. H. Dill, M. Lembo, Z. Lu, and I. Tobias. On the dynamics of rods in the theory of Kirchhoff and Clebsch. *Arch. Rat. Mech. Anal.*, **121**, 339–359, 1993.

[9] J. Coyne. Analysis of the formation and elimination of loops in twisted cable. *IEEE J. Ocean. Eng.*, **15**, 72–83, 1990.

[10] M. C. Cross and P. C. Hohenberg. Pattern formation outside of equilibrium. *Rev. Mod. Phys.*, 65, 1993.

[11] S. Da Silva and A. R. Chouduri. A theoretical model for tilts of bipolar magnetic regions. *Astron. Astrophys.*, **272**, 621, 1993.

[12] J. D. Gibbon and M. J. McGuinness. Amplitude equations at the critical points of unstable dispersive physical systems. *Proc. Roy. Soc. Lond. A*, **377**, 185–219, 1981.

[13] R. E. Goldstein and D. M. Petrich. The Korteweg–de Vries hierarchy as dynamics of closed curves in the plane. *Phys. Rev. Lett.*, **67**, 3203–3206, 1991.
[14] R. E. Goldstein and S. A. Langer. Nonlinear dynamics of stiff polymers. *Phys. Rev. Lett.*, **75**, 1094, 1995.
[15] A. Goriely and M. Tabor. New amplitude equations for thin elastic rods. *Phys. Rev. Lett.*, **77**, 3537–3540, 1996.
[16] A. Goriely and M. Tabor. Nonlinear dynamics of filaments I: Dynamical instabilities. *Physica D*, **105**, 20–44, 1997.
[17] A. Goriely and M. Tabor. Nonlinear dynamics of filaments II: Nonlinear analysis. *Physica D*, **105**, 45–61, 1997.
[18] A. Goriely and M. Tabor. Nonlinear dynamics of filaments III: Instabilities of helical rods. *Proc. Roy. Soc. Lond. (A)*, **453**, 2583–2601 1997.
[19] A. Goriely and M. Tabor. Nonlinear dynamics of filaments IV: Spontaneous looping. *Proc. Roy. Soc. Lond. (A)*, **455**, 3183–3202 1998.
[20] A. Goriely and J. Lega. Pulses, fronts and oscillations of an elastic rod. *Physica D*, **32**, 373–91 1999.
[21] N. G. Hunt and J. E. Hearst. Elastic model of DNA supercoiling in the infinite length limit. *J. Chem. Phys.*, **12**, 9329–9336, 1991.
[22] J. P. Keener. Knotted vortex filamnent in an ideal fluid. *J. Fluid Mech.*, **211**, 629–651, 1990.
[23] G. L. Lamb, Jr. Solitons on moving space curves. *J. Math. Phys.*, **18**, 1654–1661, 1977.
[24] L. D. Landau and E. M. Lifshitz. *Theory of elasticity*. Pergamaon Press, Oxford, 1959.
[25] J. Langer and R. Perline. Poisson geometry of the filament equation. *J. Nonlin. Sci.*, **1**, 71–93, 1991.
[26] A. E. H. Love. *A treatise on the mathematical theory of elasticity*. Cambridge University Press, Cambridge, 1892.
[27] A. Mielke and A. Holmes. Spatially complex equilibria of buckled rods. *Arch. Rat. Mech. Anal.*, **101**, 319–348, 1988.
[28] K. Nakayama, H. Segur, and M. Wadati. Integrability and the motion of curves. *Phys. Rev. Lett.*, **69**, 2603–2606, 1992.
[29] A. C. Newell and J. A. Whitehead. Finite bandwidth, finite amplitude convection. *J. Fluid Mech.*, **38**, 279–303, 1969.
[30] A. Newell. Envelope equations. *Lect. Appl. Math.*, 15, 1974.
[31] M. Nizette and A. Goriely. Towards a classification of Euler-Kirchhoff filaments. *J. Math. Phys.*, **40**, 2830-2866, 1999.
[32] F. Sass and Ch Bouché. *Dubbels Taschenbuch für den Maschinenbau*. Springer-Verlag, Berlin, 1953.
[33] T. Schlick and W. K. Olson. Trefoil knotting revealed by molecular dynamics simulations of supercoiled DNA. *Science*, **257**, 1110–1114, 1992.
[34] M. J. Shelley and T. Ueda. The nonlocal dynamics of stretching, buckling filaments. In *Advances in multifluid flow*s, pages 415–425. SIAM, Philadelphia, 1996.
[35] Y. Shi and J. E. Hearst. The Kirchhoff elastic rod, the nonlinear Schrödinger equation and DNA supercoiling. *J. Chem. Phys.*, **101**, 5186–5200, 1994.
[36] I. S. Sokolnikoff. *Mathematical theory of elasticity*. McGraw-Hill, New York, 1956.
[37] H. C. Spruit. Motion of magnetic flux tubes in the solar convection zone and chromosphere. *Astron. Astrophys.*, **98**, 155, 1981.
[38] J. M. T. Thompson and A. R. Champneys. From helix to localized writhing in the torsional postbuckling of elastic rods. *Proc. Roy. Soc. Lond. A*, **452**, 117–138, 1996.
[39] G. H. M. van der Heijden, A. R. Champneys, and J. M. T. Thompson. The spatial complexity of localized buckling in rods with noncircular cross section. *SIAM J. Appl. Math.*, **59**, 198-221, 1997.

[40] G. H. M. van der Heijden and J. M. Thompson. Lock-on to tapelike behaviour in the torsional buckling of anistropic rods. *Physica D*, **112**, 201–224, 1998.
[41] Y. Yang, I. Tobias, and W. K. Olson. Finite element analysis of DNA supercoiling. *J. Chem. Phys.*, **98**, 1673–1686, 1993.
[42] E. E. Zajac. Stability of two planar loop elasticas. *Transactions of the ASME*, 136–142, March 1962.